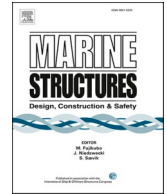




ELSEVIER

Contents lists available at [ScienceDirect](https://www.sciencedirect.com)

Marine Structures

journal homepage: www.elsevier.com/locate/marstruc

Shear lag effects on global bending moments in a long-span pontoon bridge under self-weight, traffic and environmental loads

Chenyu Luan^{a,*}, Torgeir Moan^{b,c}, Knut Andreas Kvåle^d, Zhengshun Cheng^{e,f}

^a CNOOC Renewable Energy Co., LTD, 200335, Shanghai, China

^b Department of Marine Technology, Centre for Autonomous Marine Operations and Systems (AMOS), NTNU, NO-7491, Trondheim, Norway

^c Ningbo University, 315211, Ningbo, Zhejiang, China

^d Department of Structural Engineering, Faculty of Engineering, NTNU, NO-7491, Trondheim, Norway

^e State Key Laboratory of Ocean Engineering, Shanghai Jiao Tong University, Shanghai, 200240, China

^f SJTU Yazhou Bay Institute of Deepsea Science and Technology, Sanya, 572024, China

ARTICLE INFO

Keywords:

Shear lag effect
Finite element analysis
Structural dynamic analysis
Pontoon type floating bridge

ABSTRACT

The present paper deals with a systematic study of the shear lag effect on the bending moment distribution in girders of representative pontoon-type floating bridges (PTFBs). Comparative and parametric studies for well-developed beam and linear shell models for representative structural components of a reference PTFB subject to representative static and dynamic loads, e.g. self-weight load condition, traffic loads, and wave-induced vertical dynamic loads on PTFB's pontoons are carried out. The study is partly based on a simplified, generic PTFB model, denoted GPTFB. The study shows that elementary beam element models, for which shear lag effects are not accounted for, might, to some extent, inaccurately predict the bending stiffness, eigenmode shapes and eigen frequencies of PTFBs with large width and relatively short span lengths (e.g. the ratio of span length to girder width of PTFBs is less than 7.24), while the inaccurate prediction of beam model in weak axis bending moment in girder of the PTFBs is related to the load pattern and dynamic load frequency range. A practical method is proposed to judge when caution is needed in using elementary beam model for estimating the weak axis global bending moments in girder of PTFBs. In addition, a case study presented in this paper, shows that the part of the girder near the bank abutment might be subjected to complex boundary conditions since the girder is supported by floating pontoons and bottom fixed columns. In this part of the bridge girder, a significant influence of shear lag on weak axis bending moments is observed. Further analysis by using shell elements is necessary to estimate the stresses, including the effect of shear lag, in this part of the girder.

1. Introduction

Floating bridges is a viable alternative for crossing wide and deep fjords along the coastal highway E39 in Norway [1]. The feasibility of several concepts has been analyzed to different extents [2]. In this study, a side-anchored straight pontoon type concept and an end-anchored curved pontoon type concept are considered as attractive solutions since several pontoon type floating bridges, e.

* Corresponding author.

E-mail addresses: luanchy@offshoreoil.com.cn (C. Luan), torgeir.moan@ntnu.no (T. Moan), knut.a.kvale@ntnu.no (K.A. Kvåle), zhengshun.cheng@sjtu.edu.cn (Z. Cheng).

<https://doi.org/10.1016/j.marstruc.2023.103518>

Received 17 February 2023; Received in revised form 26 August 2023; Accepted 17 September 2023

Available online 6 October 2023

0951-8339/© 2023 The Authors. Published by Elsevier Ltd. This is an open access article under the CC BY license (<http://creativecommons.org/licenses/by/4.0/>).

g. the Bergsøysund truss bridge [3], Nordhordland box girder Bridge [4], and the 520 bridge in Washington State of U.S. [5], have been built and successfully operated in decades.

The configuration of an end-anchored curved pontoon type concept for the Bjørnafjord is shown in Fig. 1. The bridge is composed of pontoons, columns and girders [6], and is subjected to self-weight, traffic and aero- and hydro-dynamic loads, which result in local and global static and dynamic load effects. It is noted that the focus in this paper is on shear lag effects and hence the vertical wave load induced responses for which the oscillating period is in between 3s and 25s and wind loads have very limited contributions.

The development of pontoon-type floating bridges (PTFBs) is built upon the knowledge and experience from long-span cable-stayed bridges and very large floating structures, while unique features of PTFBs should be approximately accounted for. To ensure structural safety, Ultimate Limit State (ULS) and Fatigue Limit State (FLS) design checks are required by relevant standards, e.g. Eurocode [7] and NORSOK N004 [8] as used in accordance with the design basis of a floating bridge concept for the Bjørnafjord crossing [9]. Wave and wind induced load effects need to be assessed by time-domain dynamic analysis considering short-term and long-term stochastic features of coupled wind and wave loads. PTFBs are modelled by combining approaches used for modelling cable-stayed bridges and offshore units, e.g. Refs. [10–17]. As a result of a trade-off in computational efficiency, accuracy, and robustness of computer codes, software such as Simo/Riflex [18,19] and Orcaflex [20] are extended and applied [21–24]. These tools were initially developed for analyzing floating structures combined with, e.g., mooring lines and risers. A representative model for a curved PTFB is described by Cheng et al. [24].

In the model of Cheng et al. [24], the columns and girders of the bridge are modelled by 2-node-12 degrees of freedom (d.o.f.s) -3D elementary beam elements with equivalent cross-sections. Global structural responses which are captured by the beam elements, in terms of sectional forces and moments and deformations, could be used as boundary conditions for a refined finite element model to determine local stresses. Alternatively, the local stresses can be determined by analytical and empirical formulae given in design standards for specific structural components. However, due to limitations of the elementary beam elements, shear lag effects on the global structural responses are not included.

The stress distribution due to bending moments in wide box beams can differ from that derived according to the elementary beam theory because shear forces exist. This has been recognized for a long time [25] and extensively studied numerically (by carrying out linear shell element finite element analysis [26,27] or by an elementary or Timoshenko beam element model with additional d. o.f. To account for shear lag effect [28–30]), experimentally [31], and analytically [32]. However, special beam elements with more d. o.f.s than the Euler-Bernoulli and Timoshenko beam elements, do not seem to be implemented in the general purpose software for static and dynamic analysis. Alternatively, the bridge girder can be designed by providing sufficient longitudinal diaphragms to reduce the shear lag effect as illustrated in Appendix A.

However, quantitative studies of the shear lag effect on bending moment distribution in bridge girders are very limited. Previous studies focus on stress distributions in the beam cross-section, and on establishing simplified methods with an effective flange width [7, 33] or a “stress increase factor” [27] to correct the stresses derived by using elementary beam theory in ULS or FLS design checks, to match the corresponding actual unevenly distributed stresses. In the previous studies relating to moment distribution, the analyzed structural components are statically determinate, e.g., simply-supported or cantilevered beams, for which the bending moment distribution is statically determinate; or clamped-end conditions with uniformly distributed loads, for which the symmetrical load pattern and boundary and slender configuration of the analyzed structural component make the shear lag effect on bending moment distribution negligible [31]. In addition, situations where the girder is statically indeterminate and the effects of external and inertial loads on the dynamic behavior are not considered in the previous studies. In Eurocode [7], it is required that the shear lag effect on stiffness of structural components shall be taken into account in the global analysis by an effective width, which is determined by the distance between each adjacent zero-bending-moment cross-section in the beams. In practice, as mentioned above, the popular cost-effective commercial computer codes based on elementary beam elements do not have the capability to account for the variation in stiffness of the global models due to shear lag. Moreover, publications on shear lag effects for stochastic dynamic problems, which involve complex response variation in time and space, are limited.

This paper aims, especially, at shedding light on the uncertainties in global bending moments that are obtained by elementary beam

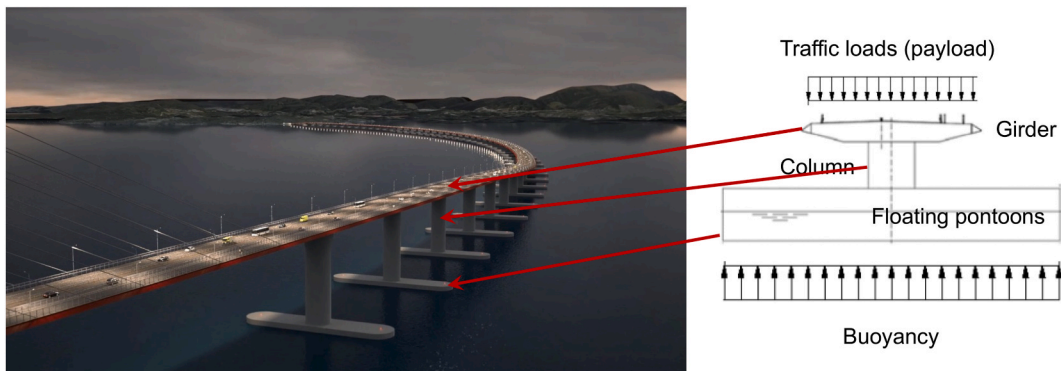


Fig. 1. A curved floating surface bridge [6].

element models for long-span PTFBs. Therefore, the effect of shear lag on the bending moment distribution in girders of a reference PTFB is systematically studied, considering representative static and dynamic loads and boundary conditions. In this study, simulated results using elementary beam elements are compared with those obtained by using converged linear shell elements. The shell element models are used for reference.

2. Description of floating bridge models

2.1. Floating bridge for fjord crossing

The floating bridge considered in this study is an end-anchored floating bridge, as shown in Fig. 1. It was initially proposed as a design for the Bjørnafjord crossing in Norway. The configuration of the floating bridge concept is shown in Fig. 2. The whole bridge structure consists of a cable-stayed high bridge part and a low bridge part. The high bridge part was designed for ship navigation while the low bridge part was supported by 46 pontoons.

Structural details of the floating bridge, including the girder, cables, columns and pontoons, are described in Ref. [34]. A coupled hydro-elastic model was developed for the floating bridge based on the modal superposition and was used to reveal the shear lag effects on the dynamic responses of floating bridge girders in Section 5.3.

To shed light on the shear lag effect on the bending moment distribution in the part of the girder of generic pontoon-type floating bridges (GPTFB), a comparative analysis is conducted by simulating the static and dynamic responses of corresponding beam and shell models for a reference structure subjected to corresponding representative loads. The reference structure is described in Section 2.2 and is used for representing the pontoon-supported low-bridge part of GPTFBs, which could be for example about 85% of the whole bridge length [35].

2.2. The reference structure

Configuration of the reference structure is shown in Fig. 3. The reference structure is a steel box girder supported by eleven columns and pontoons. Configurations and structural details of the girder, columns and pontoons of the structure are identified from preliminary design of a side-anchored straight PTFB concept and the end-anchored curved PTFB concept for the Bjørnafjord [34,35]. To highlight the shear lag effect, reasonable simplifications are implemented. Note that the pontoons of the model are allocated in a straight line.

As shown in Appendix D, the shear lag effect on the strong axis bending moment distribution of the girders of the PTFBs, (M_z , see Fig. 4 in Section 2.3.1), is expected to be negligible due to their relatively large ratios of the span length to height of the girder (the height of the girder with respect to the strong axis is the width of the girder). Therefore, the present paper focuses on weak axis bending moment distributions, (M_y , see Fig. 4), in the part of the girder supported by floating pontoons.

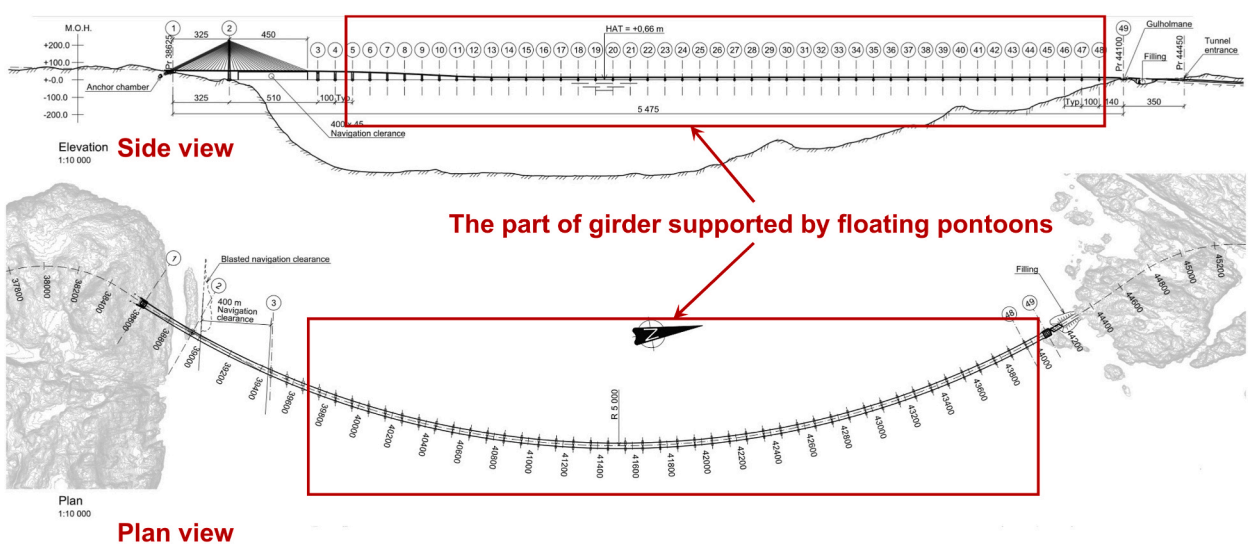


Fig. 2. Configurations of an end-anchored curved PTFB for Bjørnafjord [34].

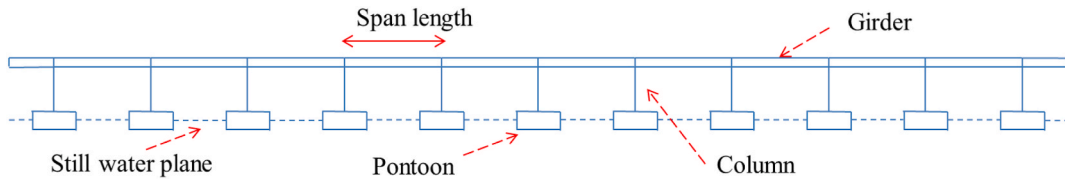


Fig. 3. Configuration of the reference structure.

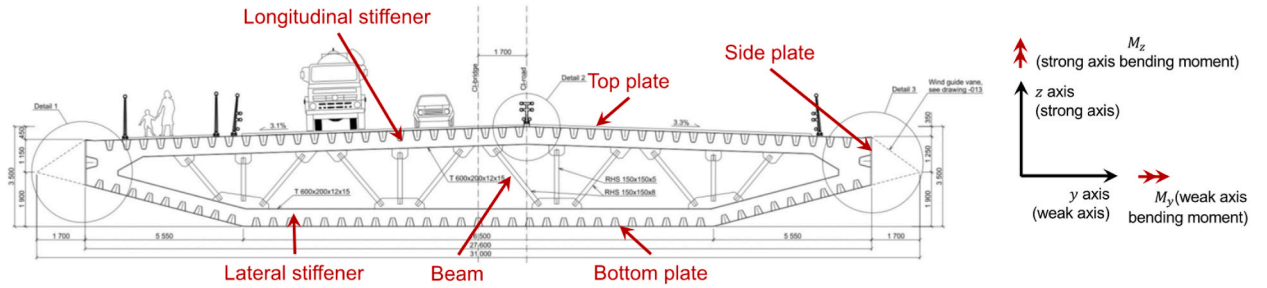
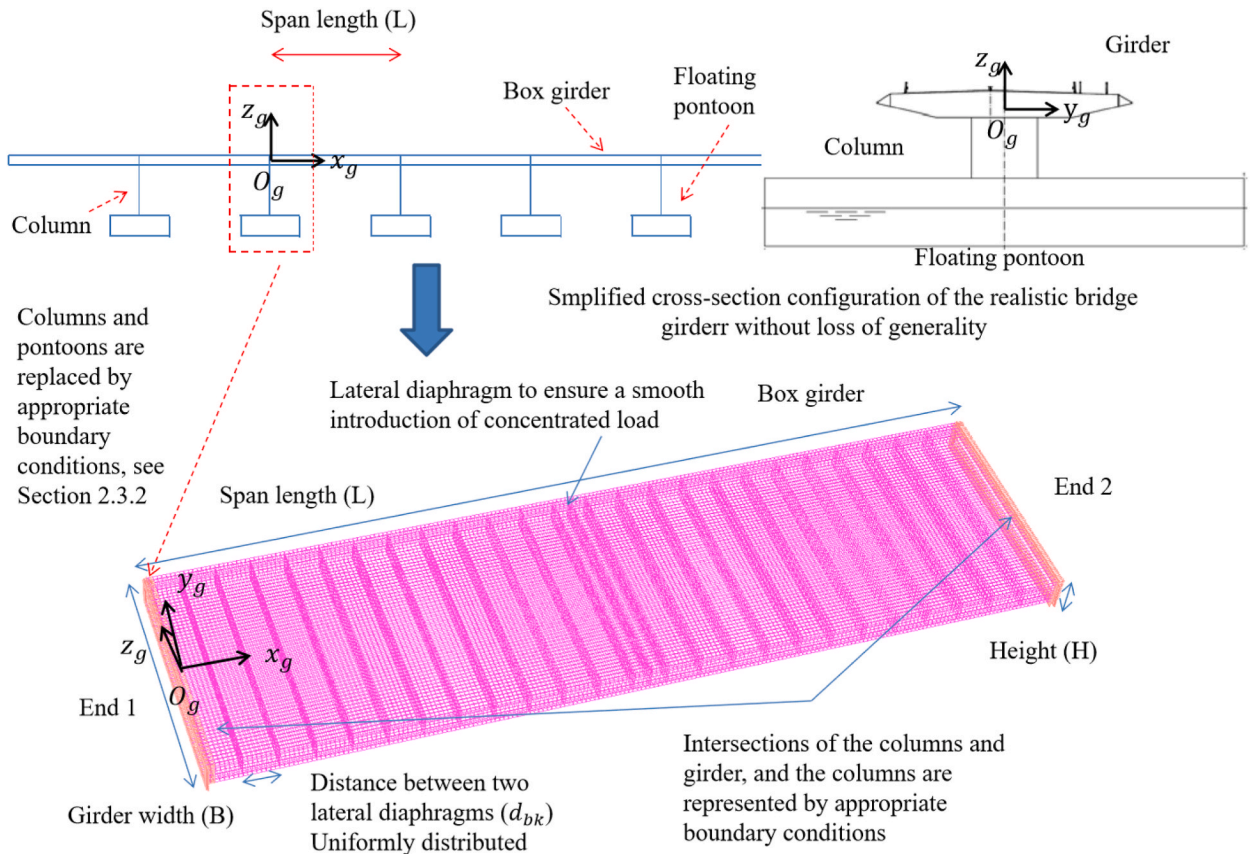


Fig. 4. Representative cross-section layout for the curved bridge [36].



**Configuration of a developed thin-walled structure
(a shell element model for a single span length of a box girder)**

Fig. 5. Illustration for the simplified cross-section configuration of the realistic bridge girder without loss of generality.

2.3. Structural details of the reference structure

2.3.1. Girder

The realistic bridge girder is continuous and, as shown in Fig. 4 [36], is composed of top, side and bottom plates, which are stiffened by longitudinal stiffeners, and lateral stiffeners and beams. However, a simplified cross-section configuration of the girder, as illustrated in Fig. 5, is applied without loss of generality in this study. The girder is simplified as a thin-walled structure with horizontal diaphragms and box-shape cross-section. The lateral stiffeners and beams are simplified by the horizontal diaphragms. Similarly, as longitudinal stiffeners, shown in Fig. 4, on top, and bottom plates of the girder have a negligible effect on shear stress distribution and shear deformation distribution in the top and bottom plates. Therefore, these stiffeners are not modelled without loss of generality for the present investigation. This is confirmed by a comparative study with and without the longitudinal stiffeners and supported by the work shown in Ref. [37]. It should be noted that when the unstiffened plates of the girder are modelled by shell element, the stiffness matrix can be badly conditioned if concentrated lateral loads are applied to investigate the local stress distribution; however, this is not a problem for the present study because in the analyzed cases shown later distributed external loads are applied and distribution of sectional forces along the girder is of interest.

In dynamic finite element analysis, the contribution of the longitudinal stiffeners on inertial loads and axial and bending cross-sectional stiffness should be appropriately accounted for. As shown later in the present paper, this can be done by adjusting the thickness and/or Young’s modulus of the plates since they have negligible effects on the shear lag effect discussed later in the present paper.

In addition, the shear stress distribution will be significantly affected by using continuous longitudinal diaphragms to connect the top and bottom plates. As an example, Figure A1 in Appendix A shows that the shear lag effect on stress distributions in the top plate of a steel box girder could be significantly reduced by adding two continuous longitudinal diaphragms to the girder shown in Fig. 4.

The part of the girder between two adjacent pontoons is defined as a single span of the girder, see Fig. 3. Consequently, the girder is composed of eleven spans. The configuration of each span is shown in Fig. 5 and is characterized by: 1) Span length (L); 2) Girder width (B); 3) Height (H); 4) Thickness of the plates and diaphragms (t) and 5) Distance between two lateral diaphragms (d_{lk}). The lateral

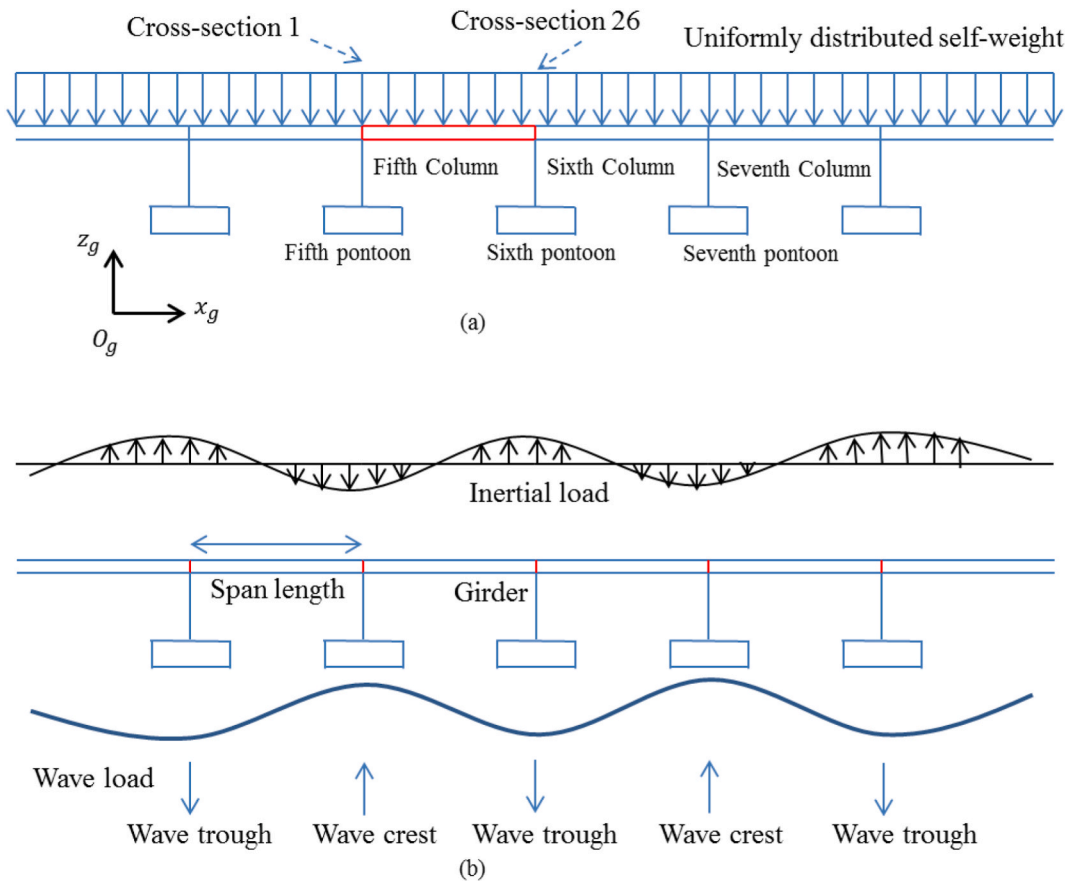


Fig. 6. Simplified illustration of load pattern on the girder subjected to uniformly distribute self-weight (a) and a representative wave excitation load (b). Note wave direction is along the bridge girder, in realistic floating bridge is subject to short-crest waves and the fluctuation of wave loads in time and space excites dynamic response that can be interpreted in terms of modal superposition.

Table 1
List of features of developed models for a single span of the girder.

	Girder width (B) [m]	Mesh size [m]	Note
MSA01	27.6	0.2	For all of the models, the span length (L) is 100 m; the web height (H) is 3.15 m; the thickness of the plates and diaphragms (t) is 0.014 m; and the distance between two lateral diaphragms (d_{bk}) is 4 m.
MSP01			
MSC01			
MSC02			
MSD01	13.8	0.1	
MSD02	0.5	0.05	H, t and d_{bk} are identical to MSC01. L is doubled to 200 m.
MSD03	0.5	0.05	
MSD04	27.6	0.2	
MSD05	13.8	0.1	

diaphragms are uniformly distributed from one end of the span to the other end except that there is always a lateral diaphragm at mid span of the girder. The plates and diaphragms are assumed to be made of steel with density, Poisson ratio and Young’s modulus specified as 7850 kg/m^3 , 0.3, and 210G Pa , respectively. The same thickness is applied to all plates and diaphragms.

Note that the dimensions, e.g. L, B, H, t, of finite element models of the reference structure shown in Sections 2.4 and 2.5 are based on [34–36] which is representative for a 4 lane GPTFBs.

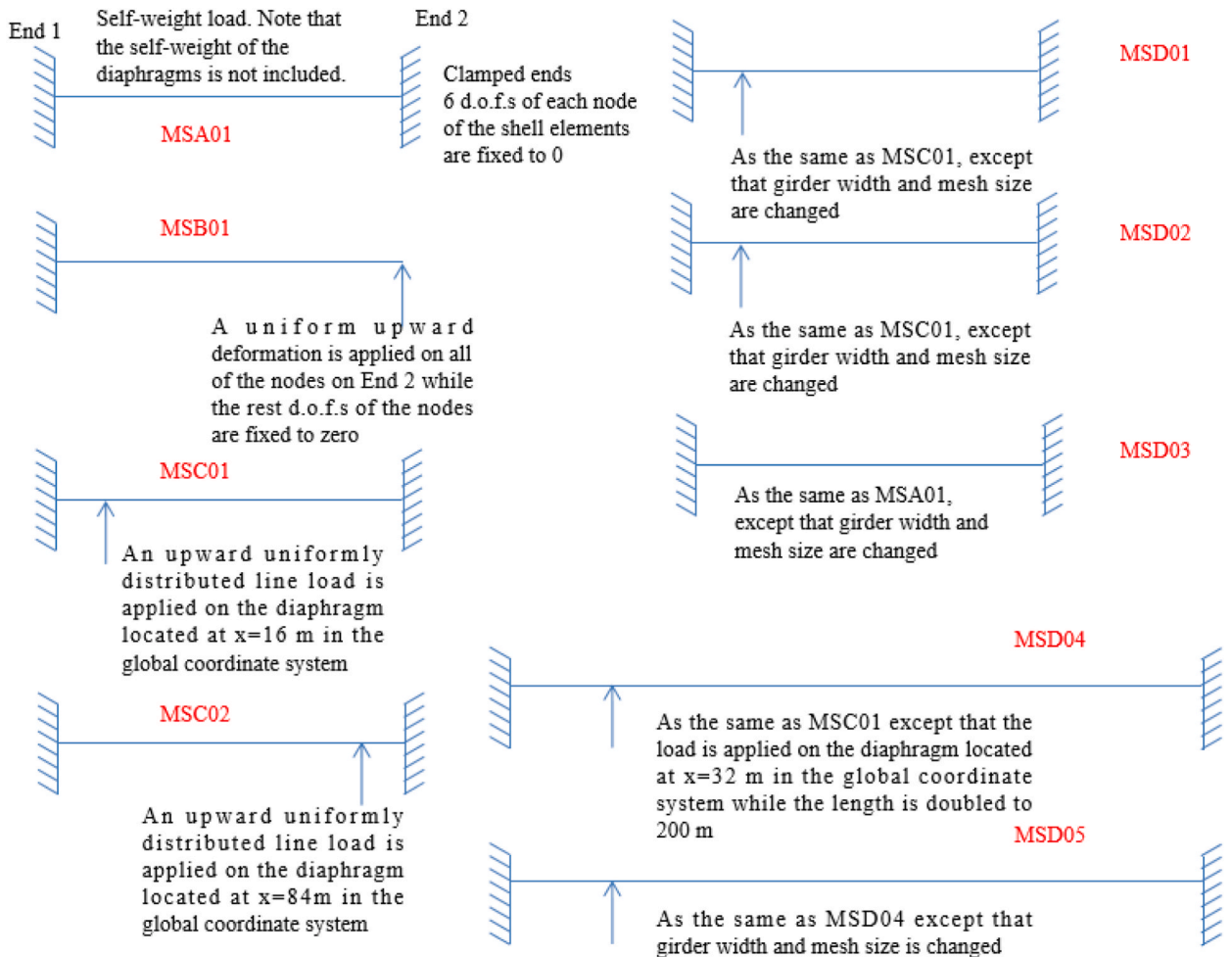


Fig. 7. Figure of load and boundary conditions of developed models for a single span of the girder. Note that each model has two end cross-sections, i.e. denoted as End 1 and End 2. The global coordinate system $O_g-x_g-y_g-z_g$ is always allocated at the geometrical center of End 1, as shown in Fig. 6 for example.

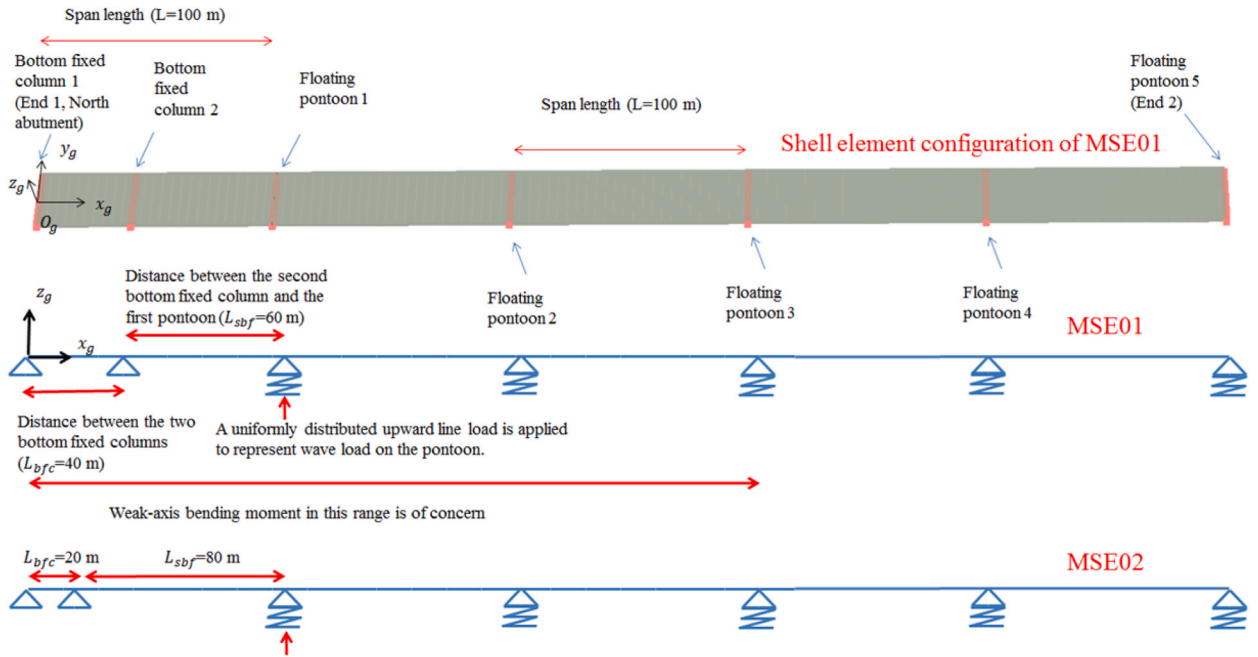


Fig. 8. Configuration of shell finite element model (MSE01) for the part of girder supported by floating pontoons and north bank abutment.

2.3.2. Columns and pontoons

In reality, the girder is supported by columns/pontoons. This fact means that there are additional diaphragms at the intersection between the columns and girder. However, as the focus of this study is on the shear lag effect relating to the weak axis bending moment distribution in the girder, the additional diaphragms, columns and pontoons are replaced by appropriate boundary conditions. A detailed analysis of the stresses in the intersection and columns is outside the scope of this study.

2.4. Finite element models of the reference structure for static analysis

2.4.1. Models for static analysis with self-weight and wave loads

Static and dynamic load effects due to self-weight and the vertical component of the wave loads on the pontoons are recognized as major sources of weak axis bending moments in cross-sections of the girder. A simplified illustration of the load pattern acting on the girder, when subjected to uniformly distributed self-weight and a representative wave excitation load, is shown in Fig. 6.

Due to the symmetrical feature of these representative load conditions and similar configuration of the girder spans of the reference structure, the shear lag effect on several spans, such as the span between the fifth and sixth columns for which the effect of boundary condition on the ends of the reference structure is negligible, could be appropriately addressed by carrying out a static analysis of the shear lag effect on a single span with appropriately defined load and boundary conditions.

Therefore, shell and beam element models for a single span with different configuration characteristic parameters, and boundary and load conditions are developed. A list of features of the developed models is given in Table 1 while boundary conditions are described in Fig. 7. The models are developed in Genie [38] and solved by Sestra [39] which is a widely used commercial general-purpose finite element program for linear structural analysis. The shell element models are based on eight-node quadrilateral curved shell elements. For the beam element models, 2-node-12-d.o.f.s-3-D elementary beam elements are used. The size of the shell elements is varied (0.2 m, 0.1 m and 0.05 m) for the different considered configurations, based on convergence tests.

Fig. 5 shows a plot of a shell element model for a span in a global coordinate system $O_g-x_g-y_g-z_g$. The end cross-sections of the span are red colored in Fig. 6(a). Due to the symmetrical feature (as shown in Fig. 6(a)), the rotational degree of freedoms in y_g direction and transformation in longitudinal directions (x_g) of nodes on the end cross-sections are fixed to zero. As mentioned in Section 2.3.2, the additional diaphragms at the intersection between the columns and the girder, and between the columns and pontoons are not modelled. Instead, in theory, the corresponding load effect should be applied to the end cross-sections. However, in practice, this load effect is modelled by fixing or applying a uniform deformation on the d. o.f.s of the nodes on the corresponding end cross-sections in direction of z_g . As checked by a sensitivity study, this practical approximation results in a negligible difference, e.g. less than 2%, in bending moment distribution compared to the analytical solution. The mesh size is selected based on a convergence test, for which the discrepancy between the results of the selected mesh size and finer mesh size is at a level that is around or less than 0.2%. The features of the beam element models are given in Table 1 and Fig. 7.

2.4.2. Models for static analysis of the bridge with complex end conditions

The girder in the floating bridge is supported by columns that are mounted on floating pontoons or fixed on the sea bed or supported on the bank. Combinations of these boundary conditions, as shown in Fig. 8, can be considered as an example of a complex boundary condition that is analyzed in this study. Static behaviour is investigated for a uniform global as well as a uniform load on one span. Static traffic load effect can be represented as the linear superposition of each uniform load on different spans.

Two shell models, i.e. MSE01 and MSE02, for the reference structure with different combinations of statically indeterminate boundary conditions are developed. Each model only includes a five-span girder (the length in total is 500 m) since the rest part of the reference structure has a negligible effect on the bending moment distribution in the range of concern (i.e. the first 300 m of the girder). The models are characterized by the distance between the two bottom fixed columns (L_{bfc}) as shown in Fig. 8 and Table 2.

MSE01 represents the part of girder supported by floating pontoons and the north bank abutment. All vertical d. o.f.s of nodes on the bottom edge of the lateral diaphragms at $x_g = 0$ m and $x_g = 40$ m are fixed to represent load effects of the supporting bottom fixed columns, while line springs (in vertical direction) are applied to the nodes on the bottom edge of corresponding lateral diaphragms to represent load effects of the supporting columns on the floating pontoons. The length of each spring line is 27.6 m which equals to girder width. The stiffness of each spring line is specified as 282 kPa, based on the mean water plane area of the corresponding pontoons. A uniformly distributed upward line load (10 kN/m) is applied on the spring line for Floating pontoon 1 to represent the “static load effect” of the wave excitation. In total, the upward load applied on the spring is 10 kN/m times girder width and equals to 276 kN.

2.4.3. Models for static analysis with traffic loads

The traffic load effect is analyzed by applying the uniformly distributed downward line load on an arbitrary position (lateral diaphragm) of MSE03, which is similar to MSE01 except that the five-span girder is subjected to uniformly distributed line springs, see Fig. 9.

2.5. Shell models of the reference structure for dynamic analysis

Three shell element models for the reference structure are developed in Abaqus [40]. Features of the models are tabulated in Table 3. Each model is composed of a girder and eleven lateral diaphragms. The girder is composed of eleven spans. The structural details of each span are identical to the model shown in Fig. 5 except for the girder width (B), thickness of the plates and Young’s modulus of the plates that are modified in the different models to result in configurations and cross-sectional bending stiffness as needed by the analyses given in later part of this paper.

For each model, the girder is supported by the eleven lateral diaphragms as shown in Fig. 10. Each lateral diaphragm is attached by a mass point with a spring and damping system to approximately account for inertial and added mass load effects, potential damping effect and fluctuation of hydrostatic pressure force induced restoring stiffness of the corresponding pontoon [41]. Corresponding d. o.f. s of the shell elements of the ends of the girder are restricted to prevent rigid-body motions of the model in horizontal plane.

Two simplifications are implemented in the shell element models: 1) structural damping is not modelled in the shell element models while frequency-dependent potential damping on each pontoon is modelled as a damper with respect to the vertical motion of the pontoon with a constant damping coefficient; and 2) gravity forces on the structure, buoyancy force on the pontoons and fluctuations

Table 2
List of features of developed models for analyzing the effect of statically indeterminate boundary conditions.

MSE01	See description in Section 2.3.2 and Fig. 8
MSE02	MSE02 is identical to MSE01 except that L_{bfc} is reduced from 40 m to 20 m

Note that the stiffness of each spring line is specified as 282 kPa.

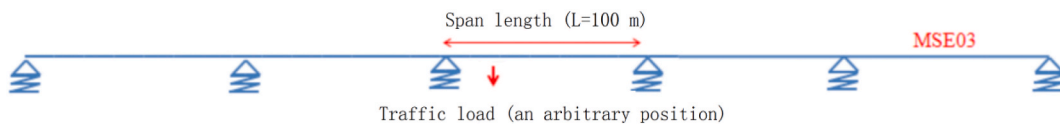


Fig. 9. Configuration of MSE03.

Table 3
List of features of developed shell element models in Abaqus for the girder with eleven spans.

	Girder width (B) [m]	Thickness of the top and bottom plates [m]	Thickness of the side plates [m]	Young’s modulus
MSH01	27.6	0.041	0.041	1.4×10^8
MSH02	1	0.041×27.6		1.4×10^8
MSH03	1	0.041×27.6		1.26×10^8

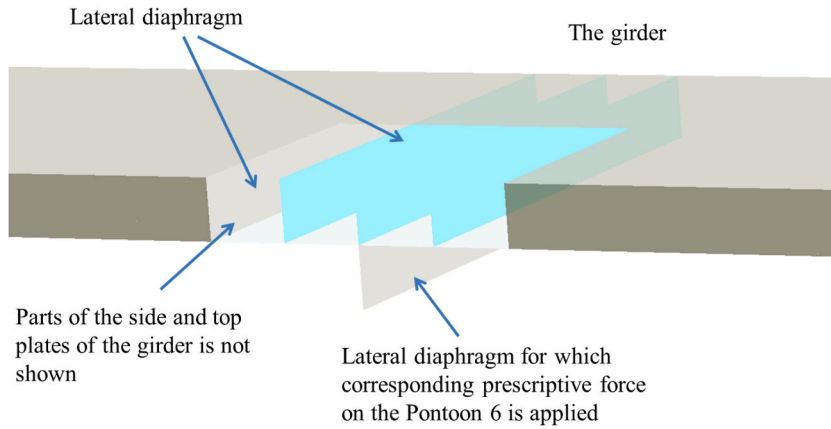


Fig. 10. Plot of part of the girder and lateral diaphragms modelled in Abaqus.

of hydrostatic pressure forces on the pontoons with respect to the rotational degrees of freedom, which affect restoring effect of the structure, are not modelled.

The simplifications make the generalized mass, stiffness and damping of the shell element model MSH01, to some extent, different from the corresponding values of the reference structure. However, the simplifications do not affect the key issues with respect to the shear lag effect. Therefore, the shell models are comparative to the beam element model described in Section 2.4 for the qualitative analysis for the shear lag effect.

3. Analysis of shear lag effects in pontoon-type floating bridges

This section deals with the effect of shear lag on responses of a representative reference floating bridge structure with relevant static and dynamic loads for a pontoon-type floating bridge with a steel box girder. The focus is on the weak axis bending moment in the bridge girder. The structure is modelled by either shell or beam models; the shell model can represent shear lag, whereas the beam model cannot. The reference structure is a girder supported by eleven evenly distributed floating pontoons as described in Section 2. The corresponding numerical models are also described in Section 2.

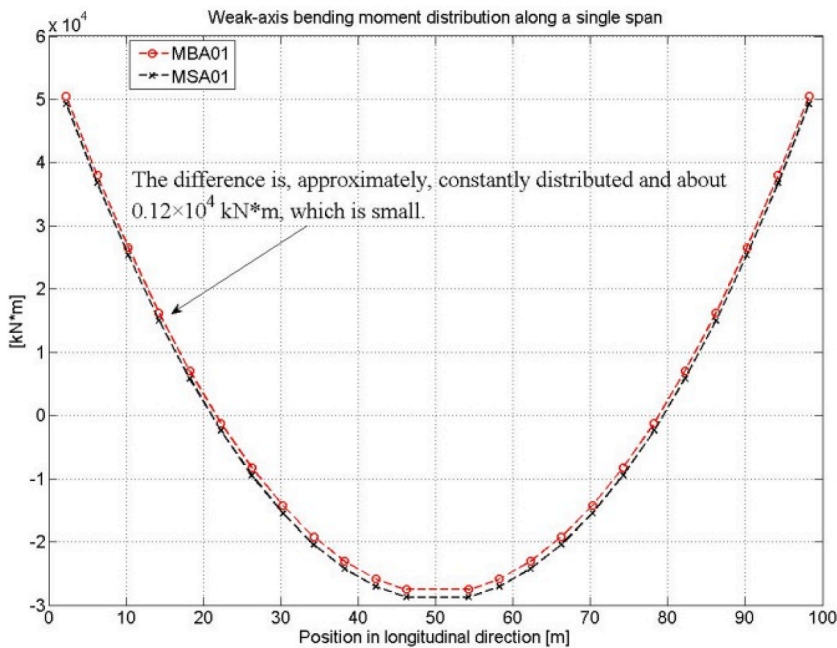


Fig. 11. Comparison of weak axis bending moments in cross-sections of the single span girder subjected to self-weight and clamped conditions given by shell and beam models (i.e. MSA01 and MBA01 described in Section 2.4).

3.1. Static response

3.1.1. Static response due to self-weight

The effect of shear lag on the weak axis bending moment in the bridge girder subjected to self-weight is investigated by comparison of the moments obtained by shell and beam models (i.e. MSA01 and MBA01 see Section 2). As the self-weight is assumed to have a symmetrical load pattern and the structure is composed of identical spans, columns and pontoons, a single span with clamped ends is used. Results in Fig. 11 show that as the shear lag effect is not accounted for, the beam model (MBA01) over-predicts the moments at the support and under-predicts the moments at the mid-span. However, in the analyzed case, the effect of shear lag is quite small. The difference between the moments in a given cross-section of the beam and shell models is about 0.12×10^4 kNm which is about 2.4% of the moment at the support of the beam model. As presented in Section 4, this effect is related to span length, girder width and height. For instance, by doubling the span length from 100 m to 200 m, the difference between the moments is decreased to be negligible.

3.1.2. Static response under complex end support boundary conditions

As shown in Fig. 8, the part of the girder supported by floating pontoons and bank abutment has indeterminate boundary conditions, which could be characterized by the distance between the two bottom fixed columns (L_{bfc}).

A comparison of static responses for the complex end support boundary condition is shown in Fig. 12. It is found that a beam element model may significantly overestimate the bending moment in the cross-section around the second bottom fixed column if L_{bfc} is relatively small.

We consider MSE01, for which $L_{bfc} = 40$ m, $L_{bfc} = 60$ m, and $L = 100$ m as a reference model. The model is subjected to an upward load acting on the first floating pontoon for which the position in longitudinal direction is 100 m in Fig. 12. The upward load is used to represent a wave load effect and/or a traffic load effect.

The comparison of MSE01 and MBE01 in Fig. 12 shows that the bending moment in the cross-sections around the second bottom fixed column is overestimated up to 13% by the beam element model. The overestimation is increased from 13% to 19% by reducing L_{bfc} from 40 m (MSE01) to 20 m (MSE02). In contrast, the overestimation is reduced by increasing L_{bfc} .

3.1.3. Traffic loads

The shear lag effect on static responses of the reference structure subjected to traffic loads is analyzed by comparing results of MSE03 and its corresponding beam model. As indicated by Fig. 9, the uniform loads, which are linear components of traffic loads, are applied on arbitrary positions (in total, 20 different positions in between the span length are analyzed). It is found that the relative difference between the corresponding shell and beam models is negligible.

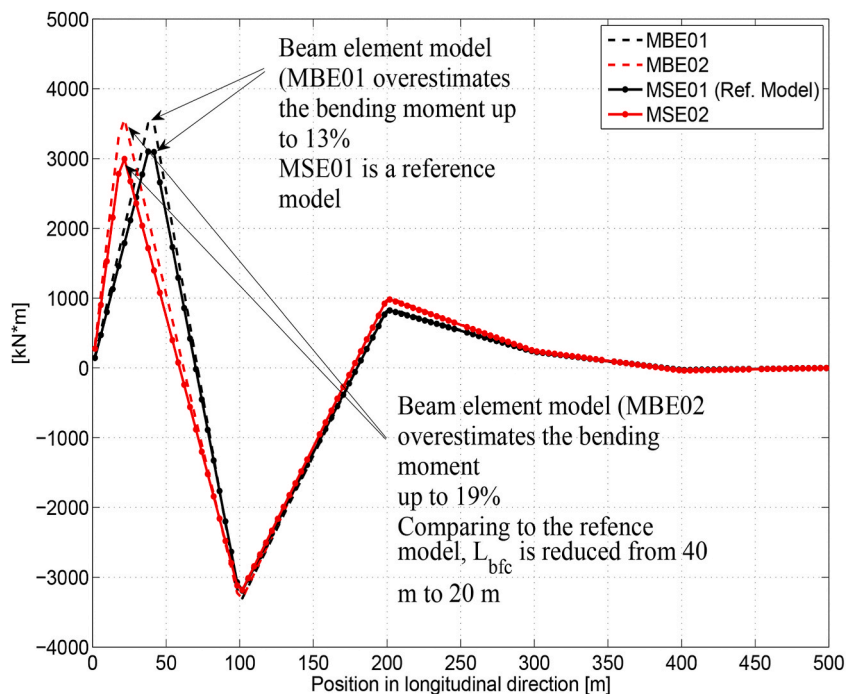


Fig. 12. Comparison between beam and shell models for the part of girder supported by floating pontoons and north bank abutment (MSE01 and MSE02 have the same geometry, boundary and load condition except the two bottom fixed supporting columns at the north end of MSE02 are closer than the counterpart of MSE01, see Fig. 8. MBE01 and MBE02 are corresponding beam models.).

3.2. Wave-induced dynamic response

This section deals with the shear lag effect when the floating bridge is subjected to wave loads. Wave excitations on the pontoons excite vertical motions of the pontoons and result in inertial loads acting on the girder. The bending moments and shear forces in the girder are particularly caused by the vertical motions of the pontoons. The character of the dynamic responses depends on the load pattern relative to the shape of the eigenmodes of the bridge and the excitation frequency relative to eigen frequencies [42].

Therefore, representative eigenmodes are discussed in Section 3.2.1. Then, Sections 3.2.2 and 3.2.3 show that the weak axis stiffness of the girder of the reference structure may be over-predicted by using elementary beam element models which do not account for shear lag effect. Consequently, the elementary beam models do not accurately capture the corresponding eigenmodes and frequencies of the girder.

Moreover, the vertical mode shapes of the bridge provide a basis for assessing the shear lag effect in each mode, as described in Section 3.2.1.

3.2.1. Representative eigenmodes

In general, floating bridges are multi-body systems for which the vibration modes can exhibit horizontal, vertical and torsional motions. This means that in each mode, some or all of the pontoons have distinct vertical motion as shown in Fig. 13. However, the present study focuses on vertical modes that could be excited by wave loads on the pontoons of the floating bridges.

Two examples of eigenmodes of a beam model for a generic pontoon-type floating bridge are shown in Fig. 13. In Mode α a given pontoon moves 180° out of phase with respect to its adjacent pontoons (a single span length). In Mode β the distance between two pontoons with 180° out of phase is three times a single span length.

In general, the eigenmodes of the beam model for the generic pontoon-type floating bridge can be characterized by effective length and eigen frequency. The effective length is defined by the eigenmode shape of the beam elements for the bridge girder, as the shortest distance between two cross-sections of the beam elements that have zero weak axis rotational deformation. For example, when the reference structure in the case study vibrates in Mode α , the effective length is 100 m. When the rotational deformation of the two cross-sections are zero, the part of the girder between them is subjected to a statically indeterminate condition for which the shear lag might have an effect on the bending moment distribution. This effect is shown in Sections 3.2.2 and 3.2.3. As mentioned in Section 3.2.2, a sensitivity study shows that the effect decreases with the increase of the effective length. Therefore, for a pontoon-type floating bridge, Mode α will likely have the largest shear lag effect since it has the shortest effective length.

3.2.2. Shear lag effects on girder stiffness

The shear lag effect can affect the bridge girder stiffness. The differences in bridge girder stiffness of the models with and without shear lag result in differences in eigenmode shapes and frequencies. This will cause differences in dynamic response when the floating bridges are subjected to dynamic loads, such as wave loads.

The effect of shear lag on the stiffness can be seen by analyzing static responses of a girder which is composed of two spans equal to the girder of the reference structure, with both ends clamped. When force is acting on the mid-span of the girder, weak axis bending moment distributions of models with and without shear lag for the girder are identical; however, deflections of the models are different and indicate the differences in stiffness. Deflections of beam element nodes and shell element nodes might not be comparable in a straightforward manner. Therefore, alternatively, the differences in stiffness are equivalently shown by comparing moment distributions of the models subjected to a unit vertical displacement on the mid-span of the girder. Therefore, comparisons of MSB01 (the

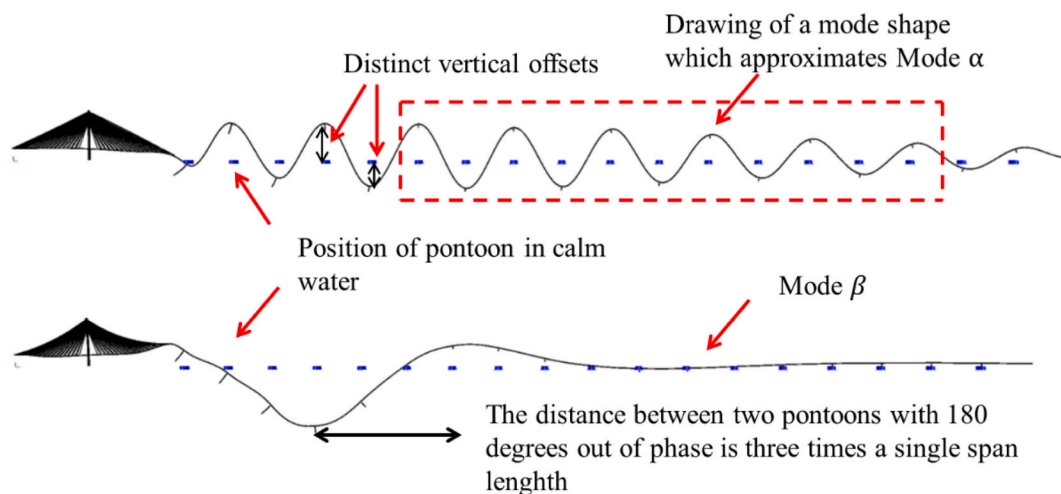


Fig. 13. Characteristics of two typical mode shapes obtained by a beam element model (without consideration of the shear lag effect) for a design of a side anchored straight floating bridge [43].

shell model) and MBB01 (the beam model) are given in Fig. 15. Boundary conditions of MSB01 and MBB01 are presented in Section 2.4.1 and shown in Fig. 7. The relative difference between weak axis bending moment in a given cross-section of MSB01 and MBB01 is about 10%, and a sensitivity study shows that the relative difference is reduced to negligible by reducing weak axis bending stiffness of MSB01 by 10% (e.g. reducing the Young’s modulus by 10%). These facts show that MBB01 over-predicts weak axis cross-section bending stiffness of the girder by 10%.

The differences in weak axis bending stiffness of the models mean differences in true eigenmode shapes and eigenmode frequencies. In the current section, the vibration in Mode α of the reference structure is used to exemplify the effect.

When the bridge girder is modelled by the elementary beam model, the eigen frequency of Mode α ($\omega_{eigen,Mode \alpha}^{beam}$) could be approximately estimated by using Eq. (1) with the effective length shown in Fig. 14. The model is composed of a pontoon, a column and a part of the girder. m represents mass of the part of the girder, column and pontoon. m_a represents added mass on the pontoon when the pontoon vibrates in the vertical direction (Z_g) with infinite frequency. k_w is the restoring stiffness in the vertical direction and is related to fluid density, gravity acceleration and water plane area of the pontoon. k_g is girder stiffness with respect to vertical wave load on the corresponding pontoon and is proportional to Young’s modulus and weak axis area moment of the girder cross-section.

$$\omega_{eigen,Mode \alpha}^{beam} \approx \sqrt{\frac{k_g + k_w}{m + m_a}} \tag{1}$$

When the bridge girder is modelled by shell model, we suggest that the eigen frequency of Mode α ($\omega_{eigen,Mode \alpha}^{shell}$) could be expressed as Eq. (2)

$$\omega_{eigen,Mode \alpha}^{shell} \approx \sqrt{\frac{\gamma_r k_g + k_w}{m + m_a}} \tag{2}$$

γ_r is a reduction factor that represents the shear lag effect on k_g and is constrained to the range [0,1]. $\gamma_r = 1$ indicates that the shear lag effect is negligible. For example, the effect of shear lag decreases with the increase of the effective length of the model (as depicted in Fig. 14). When the effective length is doubled from 100 m to 200 m, the shear lag effect is considered negligible.

As the study with respect to MBB01 and MSB01 shows that MBB01 over-predicts weak axis cross-section bending stiffness of the girder by 10%, the eigenfrequency of Mode α for shell model could be calculated by Eq. (2) with $\gamma_r = \frac{1}{1.1} = 0.91$ and this is verified by comparative analysis of dynamic responses of beam and shell models given in Section 3.2.3.

In addition, Eq. (2) shows the ratio of $\gamma_r k_g$ to k_w is affected by shear lag. This means that the relative stiffness between the girder and the restoring stiffness of the pontoon is affected by shear lag. Consequently, the relative differences between the shear forces (and bending moments) of the girder and the restoring force on the pontoon are affected by shear lag.

3.2.3. Shear lag effects for vibration in mode α

Dynamic responses of the models with and without shear lag for the reference structure vibrating in Mode α are compared in a straightforward manner by comparing dynamic responses of MSH01, MSH02, and MSH03. As described in Section 2.5, MSH01 is a simplified shell element model for the reference structure for which the shear lag effect is accounted for. MSH02 is identical to MSH01 except for a reduction of the ratio between the span width and height of the girder of the reference structure. As shown by the analysis in Appendix D, the different geometry makes the shear lag effect in the girder of MSH02 negligible. Therefore, MSH02 is considered as a reference model for which the shear lag effect is not accounted for. MSH03 is identical to MSH02 except that Young’s modulus of

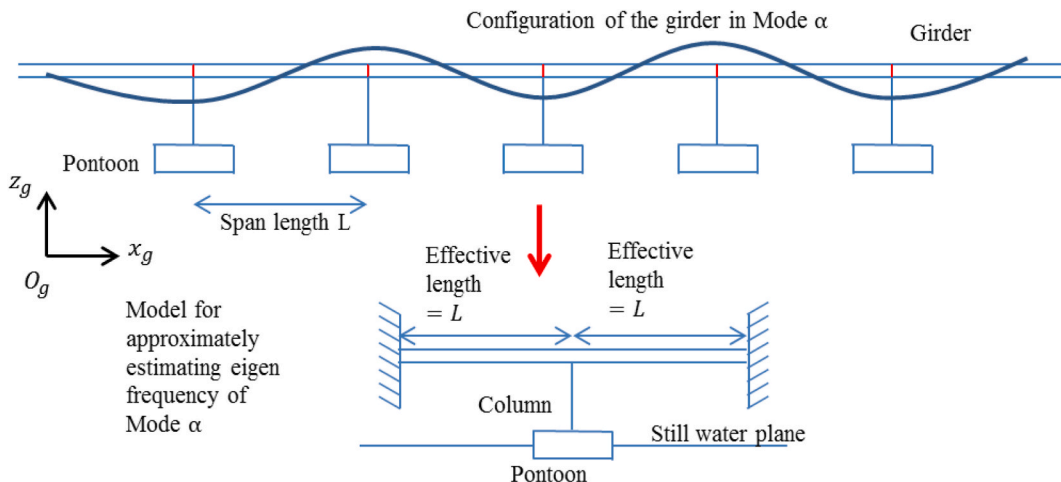


Fig. 14. Model for approximately estimating $\omega_{eigen,Mode \alpha}^{beam}$.

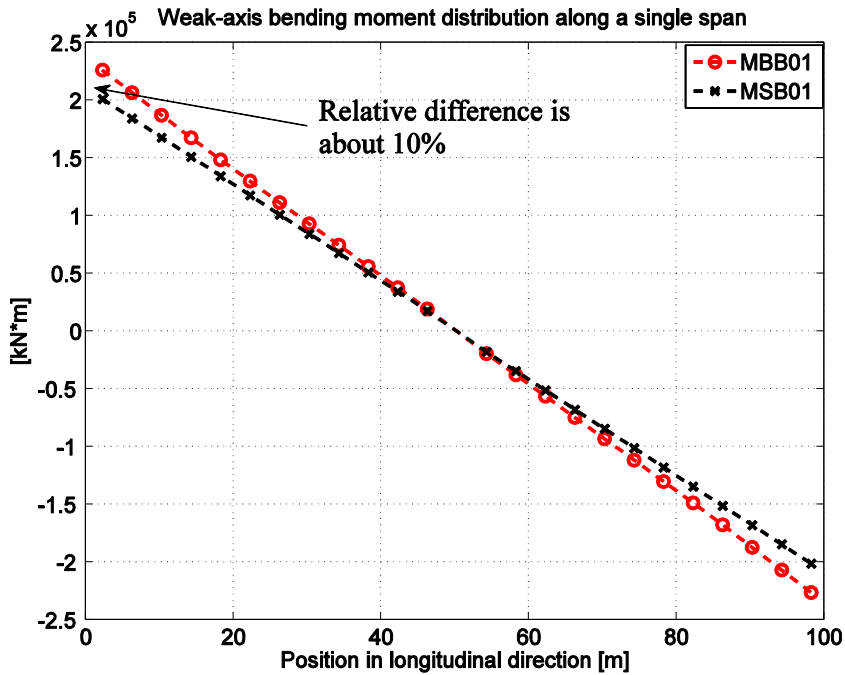


Fig. 15. Comparison of bending moments in cross-sections of a single span girder statically subjected to a uniform upward deformation on the nodes in one end of the span given by shell and beam models (MSB01 and MBB01 described in Section 2.4.1).

MSH03 is reduced by 11.4% to evenly reduce the cross-sectional bending stiffness.

Adjacent pontoons of the shell models are subjected to vertical forces that are identical in magnitude but are 180° out of phase to excite vibrations in Mode α . When a vertical force acting on Pontoon 6 is denoted as $F(t)$, the vertical forces on its adjacent pontoons, i. e. Pontoon 5 and Pontoon 7, are $-F(t)$. The transfer function of weak axis bending moments at different locations within a span is used to represent the shear lag effect. To obtain it, $F(t)$ is generated by a white noise spectrum. Consequently, transfer function modulus curves for weak axis bending moment in each of the 26 cross-sections of each shell element model with respect to $F(t)$ are analyzed. The 26 cross-sections are located between the fifth and sixth pontoons, as shown in Fig. 6.

A shear lag effect is indicated by the difference between the transfer function modulus curves of the models MSH01 and MSH02. A

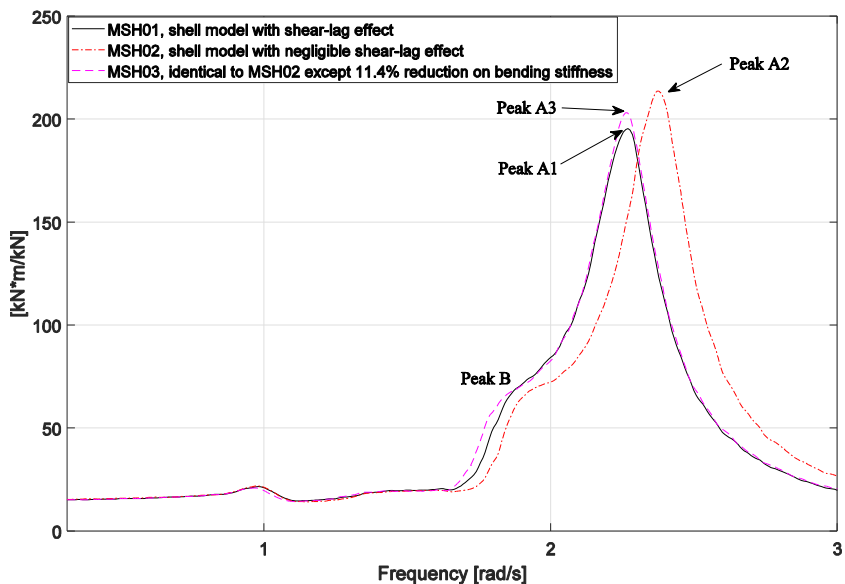


Fig. 16. Comparison of transfer function modulus curves with respect to magnitude of the vertical force on a given pontoon and weak axis bending moment in the 4th cross-section simulated by MSH01, MSH02 and MSH03 (the shell element models).

representative example is shown in Fig. 16. When the reference structure vibrates in Mode α shape and frequencies that are below 1 rad/s, the relative difference between corresponding transfer function moduli of MSH01 and MSH02 is less than 3% which is negligible; however, the relative difference is significant in frequency ranges around Peak A1 and Peak A2 since resonances in Mode α are excited at Peak A1 and Peak A2, separately, in MSH01 and MSH02. The relative difference between the frequencies of Peak A1 and Peak A2 is 4.8% and indicates that the weak axis bending stiffness of the girder and eigenfrequency of the reference structure are affected by shear lag. This is further supported by a comparison of MSH01 and MSH03, which shows that the difference between the eigenfrequency of Mode α for MSH01 and MSH02 can be eliminated by reducing Young's modulus of the girder of MSH02 by 11.4%. The reduction of Young's modulus makes weak axis bending stiffness along the girder evenly reduced by 11.4%. The difference between the transfer function moduli of MSH01 and MSH03 in the frequency range around Peak A1 is due to the shear lag effect on the eigenmode shape.

4. Accuracy of bending moment distributions simulated by elementary beam models

The shear lag might influence the distribution of bending moments about the horizontal axis (in a statically indeterminate bridge girder). In general, the influence is related to 1) structural boundary conditions, 2) structural geometrical configuration, and 3) spatial load pattern and frequency.

The present study focuses on structural boundary conditions for the part of the girders supported by many pontoons of generic pontoon-type floating bridges (GPTFBs). This means that the possible end structures, for instance, a cable-stayed bridge [34,35], are not considered. Structures at the ends of floating bridges involve complex geometries that imply the use of a more detailed shell model in the post-processing of the global response.

4.1. Behaviour under static loads

The influence of the structural geometry and load pattern on the shear lag and the accuracy of elementary beam models for GPTFBs subjected to static loads are analyzed by carrying out sensitivity studies, since linear beam and shell models are applied and the superposition principle applies.

The sensitivity studies are presented in Appendixes C and D. Appendix D shows that the difference in bending moment distributions in beam and shell models for the girder of a GPTFB subjected to static loads tend to decrease with the increase of the ratio of span length to the ratio of girder width and height, regardless of the pattern of the loads on the girder. The span length is referred to the length of girder between two adjacent pontoons. Consequently, the level of the shear lag influence on the accuracy of the beam models subjected to static loads could be characterized by span length, girder width and height.

The analysis in Appendix C shows that for the reference structure with a ratio of span length to width (L/B) of 3.62 and subjected to a static load on a given cross-section of the girder, the relative differences between the weak axis bending moments in critical cross-sections could reach approximately 10%; while the level will be reduced to 2% by doubling L/B to 7.24. Furthermore, the level decreases by increasing the ratio of girder height to width (H/B). However, the sensitivity studies show that the level is more sensitive to changes in L/B than H/B; while the variation of H/B might be limited since B is determined by the number of lanes, the ratio of B to H should be in a certain range to ensure the girder has sufficient weak axis bending stiffness relating to strength and deflection requirements.

In addition, Appendix C shows that, when the girder geometry and the static loads are symmetric to the middle cross-section of the girder, the differences between the bending moment distributions of the models with and without shear lag might be a constant value, e.g. the constant value could be 2% of the weak axis bending moment in the most critical cross-section for the reference structure subjected to uniformly distributed self-weight shown in Section 3.1.1.

Generally speaking, the differences in weak axis stiffness between models with and without shear lag vary along the girder. The case study in Section 3.2.2 and Appendix C show that, when the girder geometry is symmetric and the static load or displacement is applied on the middle cross-section of the span, shear lag has no effect on the ratio between weak axis bending moments in two given cross-sections on the girder; however, the beam element model over-predicts the weak axis sectional stiffness of the girder. The over-prediction means that the relative stiffness between the girder bending stiffness and the restoring stiffness of the water plane area of the pontoons are changed.

4.2. Behaviour under stochastic wave loads

Dynamic response of a floating bridge can be interpreted in terms of modal superposition. The case study in Section 3.2.3 shows that the mode shapes and eigen frequencies of the GPTFB are affected by shear lag, and can be characterized by effective length, girder width and height.

For a given eigenmode of a beam model, the effective length is determined on the basis of the eigenmode shape and is defined as the shortest distance between two cross-sections that have zero weak axis rotational deformation. For example, when the reference structure vibrates in Mode α , the effective length is 100 m. Mode α is identified as the most critical mode shape since it has the shortest ratio of effective length to girder width, which is 3.62. By increasing the ratio to 7.24, which is the ratio of 2 times span length to girder width, shear lag influence is reduced to a negligible level.

5. Importance of shear lag on the accuracy of beam model bending moment distributions: practical recommendations

5.1. General

Sections 5.2 and 5.3 focus on practical criteria for identifying situations for which shear lag influence on accuracy of the bending moment distribution simulated by elementary beam models for generic pontoon-type floating bridges (GPTFBs) is negligible. The practical criteria are applicable to the part of girders supported by a large number of pontoons of GPTFBs.

5.2. Static cases

The distance between pontoons (span lengths) of current floating bridges is typically in the range of 100–200 m, whereas the girder width is determined by the number of route lanes. Consequently, the ratio of span length to girder width for a 4-lane GPTFB would typically be in the range between 3.62 and 7.24. The shear lag influence on GPTFBs in this range has been analyzed by the sensitivity studies of the reference structure. It is noted that the shear lag influence is related to the ratio of girder width to height as well.

Based on the analysis results of the reference structure and the aim to make the relative difference between critical weak axis bending moments given by the beam and shell models negligible (below 2%), cases (in static loads) for which shear lag influence on the accuracy of beam models could be negligible are summarized in Table 4.

5.3. Dynamic cases

5.3.1. Criterion for identifying critical eigenmodes with respect to shear lag effect

As shown in Sections 3.2.2 and 3.2.3, the accuracy of dynamic responses of the bridge girder modelled by elementary beam models might be affected by shear lag effect since shear lag has an influence on eigenmode shape and frequency. As indicated in Section 4.2, the eigenmodes of a GPTFB can be classified into two groups, e.g. Noncritical Mode Group (NMG) and Critical Mode Group (CMG), based on a criterion such as the ratio of the effective length of each eigenmode to girder width. The criterion is tabulated in Table 5.

The shear lag effect does not need to be accounted for if the GPTFB does not have eigenmodes in CMG.

This is a conservative criterion since the influence of shear lag on accuracy of beam element models can still be negligible if the eigenmodes in CMG are not excited. To clarify this issue the modes that contribute to the dynamic response need to be determined. This contribution depends on the eigenfrequency and mode shape relative to the load variation in time and space, as discussed in the next section.

5.3.2. Application of modal superposition to identify contributions of eigenmodes

A convenient way to characterize the shear lag effect is to refer to its effect in each mode. Commonly time domain approaches are applied in the response analysis of floating bridges. Then system identification methods can be used to determine the contribution to the response from different modes. Relevant applications of such methods can be found in Refs. [44–46]. However, in this study, the dynamic response of PTFBs exposed to stochastic wave excitation is estimated by the modal superposition method, which is well established, e.g. Ref. [3]. In this method, the whole bridge is divided into two substructures, i.e. a finite element model and a hydrodynamic model. The finite element model that excludes the frequency-dependent added mass and potential damping of pontoons can provide the dry mode shapes, mass and stiffness matrices of the bridge. The hydrodynamic model provides the frequency-dependent added mass and potential damping of pontoons.

Relevant dry eigen modes are selected to form the modal transformation matrix $[\varphi_0]$. $[\varphi_0]$ is used to transform between the dry generalized coordinates $\{y\}$ and the physical degrees of freedom $\{u\}$, as follows:

$$\{u\} = [\varphi_0] \{y\} \quad (3)$$

Table 4

Cases for which the shear lag influence on accuracy of beam models subjected to static loads is negligible.

	Criterion
Case 1	The ratio of span length to girder width of GPTFBs is larger than 7
Case 2	The relative differences in weak axis stiffness of shell models with and without shear lag for a single span of bridge girder are less than 2%. The relative differences in weak axis stiffness of the models can be shown by the relative difference of weak axis bending moments in cross-sections of the single span when a unit displacement in the vertical direction is applied on one end of the span while the other end is fixed. It is noted that the applied displacement results in constantly distributed shear force in the span; the models with and without shear lag have the same bending stiffness. The model without shear lag means that the model has a very large ratio of span length to girder width, e.g. above 100. Ideally speaking, when the shear modulus is zero, there is no difference in bending moments between the models with and without shear lag.

Note.

The two cases are referred to the part of girder supported by many pontoons of GPTFBs subjected to static loads.

In reality, length, mass and stiffness of girder spans might vary within a certain range, e.g. 20%, the variations do not have a significant effect on the applicability of the criteria for the two static cases.

The influence of shear lag effect on bending moment distribution in girders of 2-lane-GPTFBs is expected to be negligible as the corresponding ratios of span length to girder width are expected to be more than 7.

Table 5
Criterion for identifying critical eigenmodes with respect to shear lag effect.

	Criterion	Consequence	Note
Noncritical Mode Group (NMG)	The ratio of corresponding effective length of the eigenmode to girder width is larger than 7	Shear lag has negligible effect.	The criterion is objected to identify the eigenmodes for which relative differences in weak axis stiffness of shell and beam models could be larger than 2%. The criterion can be definitely relaxed if uncertainty due to shear lag is accepted.
Critical Mode Group (CMG)	The ratio of corresponding effective length of the eigenmode to girder width is less than 7	Shear lag might have a significant effect	The criterion and consequences in the table are supported by the work shown in Section 3.2.2, Section 3.2.3 and the sensitivity studies in Appendix C and D.

The frequency-dependent added mass and potential damping matrices of pontoons are also transformed to dry generalized coordinate system by using $[\varphi_0]$, to form a complete linear model of the floating bridge. The resulting system of frequency-dependent equations of motion will not be diagonal as the modal transformation matrix is orthogonal with respect to the dry system matrices only. However, as long as enough dry modes are included, the solution will be accurate; the dry modes are a very efficient and appropriate coordinate basis also after the inclusion of the hydrodynamic contributions.

By employing the power-spectral density method, the response of the bridge is predicted, with respect to the dry generalized coordinates $\{y\}$. Due to the linear nature of the approach, the superposition of weak axis moment distributions from each dry mode i , $M_{y,i}(x)$, can provide the full bending moment as follows:

$$M_y(x, t) = \sum M_{y,i}^{CMG}(x)y_i^{CMG}(x, t) + \sum M_{y,j}^{NMG}(x)y_j^{NMG}(x, t) \quad (4)$$

The relative contribution of modes in the CMG can thus be assessed by comparing the full bending moment $M_y(x, t)$ with the following summation:

$$M_{y,i}^{CMG}(x, t) = \sum M_{y,i}^{CMG}(x)y_i^{CMG}(x, t) \quad (5)$$

The dry modes do not convey the true natural frequencies and damping of the system's modes. To better describe the behaviour of the bridge at resonance, the system matrices expressed using the coordinate basis given by the dry modes are therefore used to conduct a second eigenvalue solution. As the hydrodynamic added mass and damping are frequency dependent, iteration is required [3]. This implies that the modal solution obtained merely characterizes the modes at resonance. The eigenvalue solution results in a modal transformation matrix $[\psi]$ that transforms the true generalized coordinates $\{q\}$ to dry generalized coordinates $\{y\}$, as follows:

$$\{y\} = [\psi]\{q\} \quad (6)$$

Therefore, the physical degrees of freedom $\{u\}$ are related to the true generalized coordinates $\{q\}$ as follows:

$$\{u\} = [\varphi_0]\{y\} = [\varphi_0][\psi]\{q\} = [\varphi]\{q\} \quad (7)$$

The resulting mode shapes in $[\psi]$ reveal the relative contributions of all dry modes, which when combined with $[\varphi_0]$ yields the combined mode shapes at resonance. This is utilized in the grouping of modes as either CMG or NMG, which is needed for the assessment of the importance of shear lag in Eqs. (4) and (5).

As the eigenmodes are identified on the basis of an elementary beam element model of the bridge, the established bending moments do not account for the shear lag effect. However, if dynamic responses are dominated by modes in the CMG, as shown in Tables 5 and it means shear lag effect might have a significant influence on the dynamic response.

It should be noted that this approach is based on the linear superposition principle. Previous studies on dynamic responses of pontoon-type floating bridges showed that structural dynamic responses have a fairly linear behavior [47], indicating the applicability of the modal superposition method. Besides, the quality of the results relies heavily on the inclusion of a sufficient amount of modes that were used to describe the full system.

5.3.3. Case study

The results of a case study for analyzing the contributions of the modes in the CMG on dynamic weak axis bending moments in the girder of the end-anchored curved PTFB for the Bjørnafjord [34] in short-crested waves are presented in Appendix B. Contributions of CMG on the fatigue damage and extreme responses are analyzed.

The contribution of the CMG to fatigue damage associated with weak axis bending moments due to a narrow-band Gaussian response is represented by the third order of the standard deviation of weak axis bending moments, e.g. Ref. [42]. The case study shows that the modes including the shear lag effect in CMG could have a considerable contribution on dynamic weak axis bending moment in long-term wave loads. As a result, the limitation of the elementary beam theory with respect to the shear lag effect can result in large uncertainty in fatigue damage assessment for the positions for which the fatigue damage is dominated by the weak axis bending moments.

In addition, the relative importance of the contribution of the modes in CMG on dynamic of the weak axis bending moment in extreme waves selected from the 100-year contour line of the curved bridge tends to decrease with the increase of the peak wave period (T_p). Considering the condition with $T_p = 5$ s in Table B1, which yields the largest maximum, the CMG contributes 23% of the standard deviation (STD) of the dynamic. This means that, even if the elementary beam model underestimates the standard deviation of the

dynamic vibration of the modes in CMG by 50%, the beam model might only underestimate the STD of the responses, which include the contribution of full modes, by 11.5%.

While it should be emphasized that the actual uncertainty depends on the relative magnitude of vertical and horizontal bending moments, axial force and local traffic load effects to fatigue.

5.4. Discussion

This section provides a procedure for assessment of importance of the shear lag effect on the accuracy of weak axis moment distribution by using elementary beam theory. The effect of shear lag on the moment distribution is based on the effective length to girder width and reference to vertical eigenmodes. The eigenmodes are classified as critical and noncritical. Critical modes include those with an “error” of 2% due to shear lag based on a comparison against shell element models. This implies that critical modes are those with an effective length to girder width of about 7. Clearly, by relaxing the accuracy the range of noncritical modes is increased. The modal superposition method is then applied to evaluate the relative contribution of the critical mode group to the weak axis bending moment; accordingly, the uncertainty in the estimate of weak axis moment by the elementary beam theory can be approximately obtained, especially the extreme response and fatigue damage for the ULS and FLS design checks, respectively.

If the shear lag effect is found to be too large, a more accurate analysis by developing shell element models is needed. Instead of developing shell and beam models for the whole bridge, representative structures, which may be composed of several representative spans and pontoons and appropriately designed boundary conditions, are recommended for the purpose of reducing the computational cost. The work presented in Section 3.2.3 is an example for analyzing shear lag effect on dynamic responses of the reference structure vibrating in Mode α . As shown in Fig. 16, when Mode α vibration is excited while the excitation frequency is lower than 1 rad/s, the relative differences in weak axis bending moments of the models with and without shear lag are negligible (no more than 3%), while significant differences are observed in the frequency range around eigenvalue of Mode α since 1) the eigen frequency is over-predicted by the model without modeling for shear lag, 2) shear lag has an influence on mode shape and 3) damping varies in frequency.

The assessment procedure provides a quick and easy way for judging if elementary beam theory is acceptable with respect to the concern of accuracy of weak axis moment distribution and shear lag effect.

6. Conclusions

This paper extends the shear lag study with respect to statically indeterminate boundary conditions and influence on static and dynamic behavior that are relevant to generic pontoon-type floating bridges (GPTFBs) and finds that:

- Due to shear lag, bridge girder stiffness against weak-axis bending moment is different to elementary beam theory. This means elementary beam element models for bridge girders of PTFBs, for which shear lag effects are not accounted for, might, to some extent, inaccurately predict the bridge girder stiffness, eigenmode shapes and frequencies, and bending moments in bridge girders of PTFBs with large width and relatively short span lengths (e.g. the ratio of span length to girder width of PTFBs is less than 7.24).
- The level of shear lag influence in bridge girder stiffness of PTFBs could be characterized by span length, girder width and height. The level of shear lag influence decreases by increasing the ratio of span length to width (L/B) and/or the ratio of girder height to width (H/B).
- The inaccurate extent of each eigenmode shape and frequency predicted by using elementary beam model for the PTFBs, which is due to shear lag influence, could be characterized by the ratio of girder height to width (H/B) and the ratio of effective length to girder width for which the effect length is defined as the shortest distance between two cross-sections that have zero rotational deformation with respect to weak axis in the eigenmode shape.
- The shear lag influence in weak-axis bending moment distribution is related to 1) structural boundary conditions, 2) structural geometrical configuration (L/B , H/B and the ratio of effective length to girder width), and 3) spatial load pattern and frequency.

Comparative and parametric studies for well-developed beam and linear shell models for representative structural components of a reference 4-lane-PTFB subject to representative static and dynamic loads, e.g. self-weight load condition, traffic loads, and wave-induced vertical dynamic loads on PTFB's pontoons are carried out. The study is partly based on a simplified, generic PTFB model, denoted GPTFB. The major observations are highlighted as follows:

- Regarding self-weight load condition, a constant difference in bending moment distributions of the models with and without shear lag are observed although the level of the difference is very small (the critical relative difference is about 2%).
- Regarding traffic load condition, the differences in bending moments induced by traffic loads are very small as well.
- Regarding dynamic wave load conditions, the shear lag affects bridge girder stiffness and results in differences in eigenmode frequency and shape between beam and shell models. A case study shows the elementary beam model over-predicts girder stiffness of the reference structure in a level of 10% and over-predicts eigen frequency of Mode α in a level of 4.8%.

A case study to estimate the shear lag effects on the distribution of dynamic weak axis bending moments in the girder of an end-anchored curved pontoon-type floating bridge for the Bjørnafjord in Norway in short-crested waves is carried out. The case study shows that limitation of the elementary beam theory with respect to the shear lag effect can result in large uncertainty in fatigue damage assessment for locations for which the fatigue damage is dominated by the weak axis bending moments. The uncertainty in

extreme response is much more moderate since the contribution to the extreme responses of the modes affected by shear lag is relatively small.

A practical method based on L/B and the ratio of effective length to girder width is proposed to judge when caution is needed in using elementary beam model for estimating the weak axis global bending moments in the girder of GPTFBs as shear lag effect needs to be considered for static and global dynamic analyses. Generally speaking, shear lag influence is negligible if the ratios are above 7, which aims to limit the shear lag effect on bridge girder stiffness to a level of less than 2%.

The criterion is applicable to GPTFBs which might have 2–6 lanes. For GPTFBs designed for five or more lanes, additional longitudinal diaphragms are recommended to effectively limit the shear lag effect on stress and bending moment distributions. If shear lag effects on the moment distribution are not acceptable, and a conservative “safety” factor or use of more longitudinal diaphragms, imply unacceptable costs, further analysis based on combining shell and beam models would be necessary.

In addition, the part of the girder near the bank abutment might be subjected to complex boundary conditions since the girder is supported by floating pontoons and bottom fixed columns. In this part of the bridge girder, a significant influence of shear lag on weak axis bending moments is observed. Further analysis by using shell elements is necessary to estimate the stresses, including the effect of shear lag, in this part of the girder.

Declaration of competing interest

The authors declare that they have no known competing financial interests or personal relationships that could have appeared to influence the work reported in this paper.

Data availability

The data that has been used is confidential.

Acknowledgements

The authors acknowledge the financial support provided by Norwegian Public Roads Administration (NPRA) and in parts by the Research Council of Norway through the Center for Ships and Ocean Structures (CeSOS) and Centre for Autonomous Marine Operations and Systems (AMOS), at the Department of Marine Technology, NTNU, Trondheim, Norway, and Ningbo University, Ningbo, Zhejiang, China. The fourth author would like to thank the support by the National Natural Science Foundation of China (No 52201330).

Appendix A

This appendix gives an example for which the influence of shear lag effect on stress distribution could be reduced by introducing an additional longitudinal diaphragm into the girder.

Figure A1 shows axial stress distributions in top plate in cross-section at $x_g = 21.75$ m of the girder of MSE02 with and without two additional longitudinal diaphragms. Note that the stresses are averaged stresses with respect to thickness of the top plate.

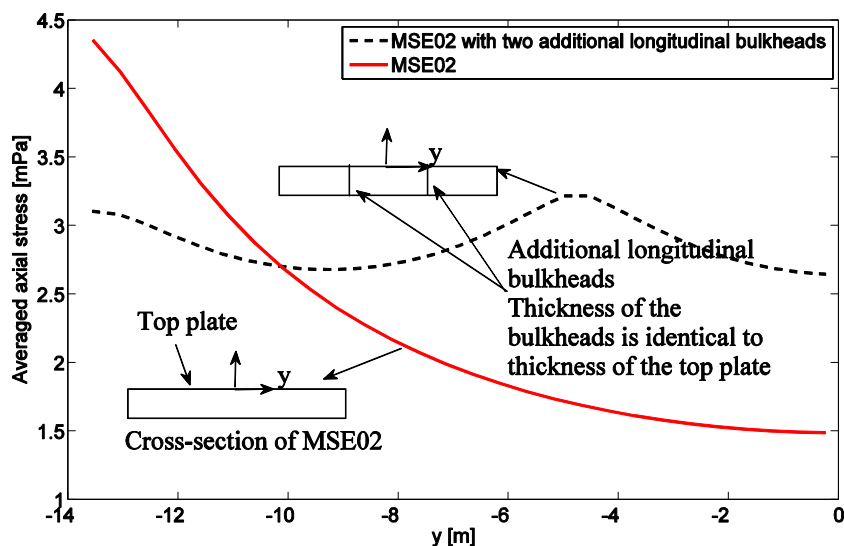


Fig. A1. Averaged axial stress distribution in top plate of cross-sections at $x_g = 21.75$ m of MSE02 with and without additional longitudinal diaphragms.

Appendix B

The first 200 eigenmodes of the end-anchored curved PTFB for the Bjørnafjord [34] are identified by eigenmode analysis based on an elementary beam model for the curved bridge. The eigenmodes, for which the ratio of effective length to girder width is less or close to 3.62 are identified as critical modes and classified into Critical Mode Group (CMG), while the other eigenmodes are classified into Noncritical Mode Group (NMG).

As shown by Eqs. (3) and (4) in Section 5.3, by implementing a modal superposition method, M_y and M_y^{CMG} are calculated and compared to show the contribution of the critical modes on weak axis bending moment in a given cross-section of the girder of the curved bridge in short-crested waves with different mean wave incident directions and long-term and extreme wave conditions. The mean wave incident directions are shown in Figure B1.

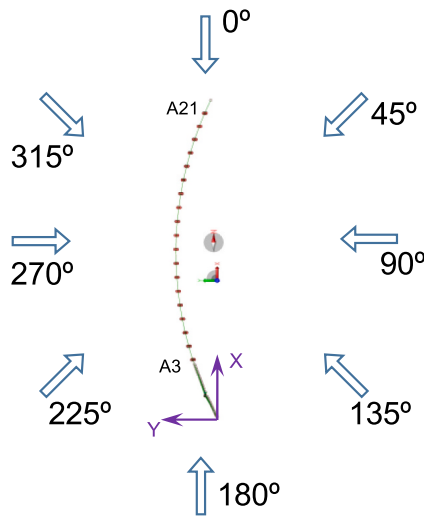


Fig. B1. The bridge with directions of incident waves [24].

The joint environmental condition of the site is developed on the basis of about 16-year simulated wave data by using the SWAN (Simulating Waves Nearshore) model. A total of 134,376 pairs of H_s and T_p with a duration of 1 h was used to derive the joint distribution and 100-year contour line of H_s and T_p . The distribution of H_s and T_p from the simulated data is shown in Figure B2. It shows that most T_p of the environmental conditions are in the range from 1.3s to 3s.

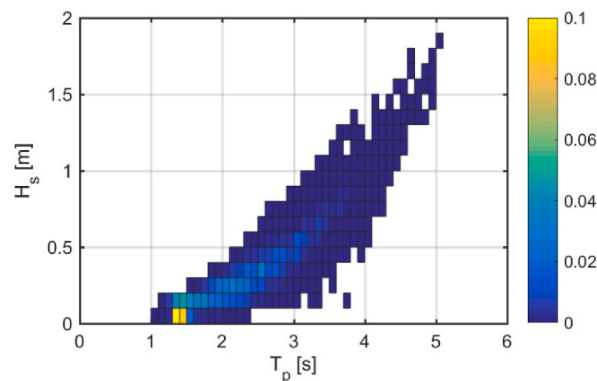


Fig. B2. Long-term distribution of H_s and T_p of the environmental conditions [48].

Comparisons show that the contributions of the critical modes depend on wave peak period (T_p) and mean wave incident direction. By analyzing the environmental conditions of the site, waves mainly come from three directions: northwest (about 315°), southwest (about 210°) and east (about 90°) due to the local topography [49]. Waves from northwest have a much larger significant wave height than those from southwest and east. Therefore, the 315° wave direction is identified as the critical direction. Besides, since waves from northwest dominate the wave conditions at the site, it is assumed in this study that waves from northwest have a similar long-term distribution as those demonstrated in Figure B2. The assumption is applicable as the focus is on showing the contribution of CMG in the standard deviation of weak-axis bending moment in realistic long-term environmental conditions rather than quantitatively calculated fatigue damage

Consequently, the contribution of the critical modes on long-term and extreme responses in waves from 315° are analyzed as

follows.

B.1 Contribution of critical modes on fatigue damage due to weak axis bending moments

If the SN curve can be expressed by $N=K S^{-m}$ and the short-term distribution of stress ranges, S (related to the weak axis bending moment) follows a Rayleigh distribution, the fatigue damage D is proportional to σ_i^m , e.g. Ref. [42]. For $m = 3$, the relative fatigue damage \bar{D} is calculated by using Eq. (B1)

$$\bar{D}(x) = \frac{n_i \sigma_i^3(x)}{\sum_{i=1} n_i} \tag{B1}$$

where σ_i^3 is the 3rd order of the standard deviation of the weak axis bending moments in the cross-section at location x of the girder in environmental condition i . n_i denotes the occurrence of the environmental condition i and $\sum_{i=1} n_i = 134376$ induced by weak axis bending moments in the cross-sections of the girder. Consequently, limitation of the elementary beam theory with respect to the shear lag effect can result in large uncertainty in fatigue damage assessment for the positions for which the fatigue damage is dominated by the weak axis bending moments.

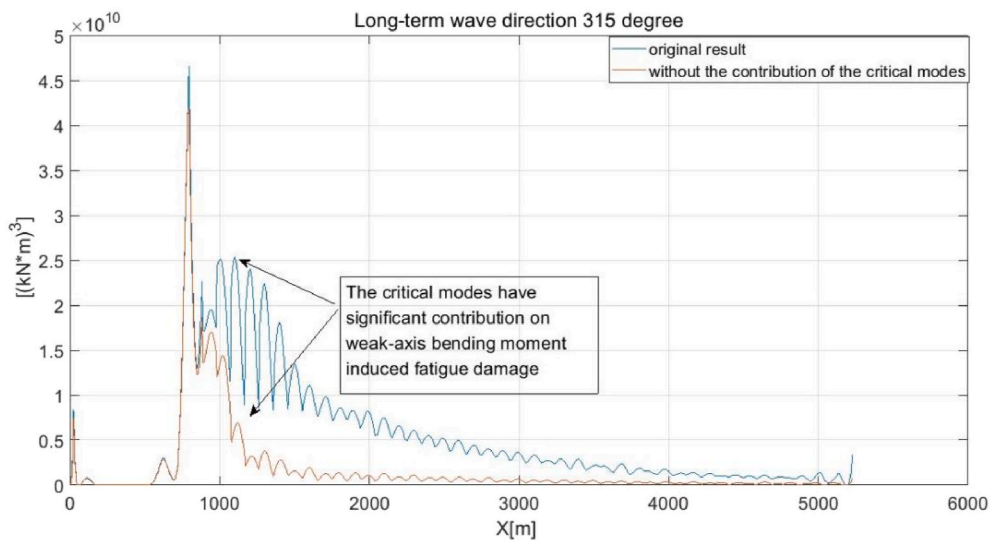


Fig. B3. Comparison of the third order of the standard deviation of weak axis bending moments in cross-sections on the girder with respect to the long-term environmental condition with and without the critical modes.

B.2 Contribution of critical modes on extreme weak axis bending moment

Dynamic responses in extreme environmental conditions selected from the 100-year contour line are analyzed. The contour line is shown in Figure B4 while the analyzed environmental conditions are tabulated in Table B1.

Table B1
environmental conditions selected from the 100-year contour line [48].

EC	Hs [m]	Tp [s]
1	0.5	2
2	0.7	2.5
3	0.96	3
4	1.2	3.5
5	1.6	4
6	1.83	4.5
7	2.07	5

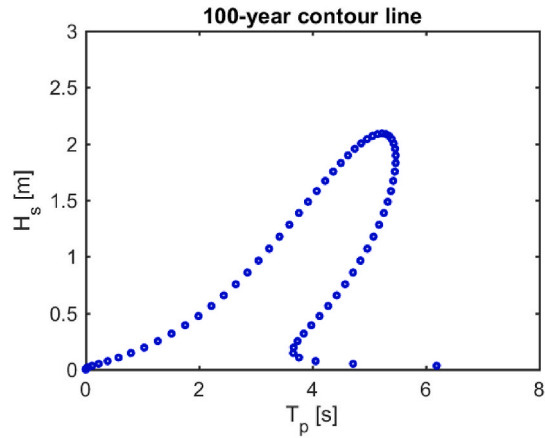


Fig. B4. 100-year environmental contour line [48].

Some representative results are given in Figures B5-B7.

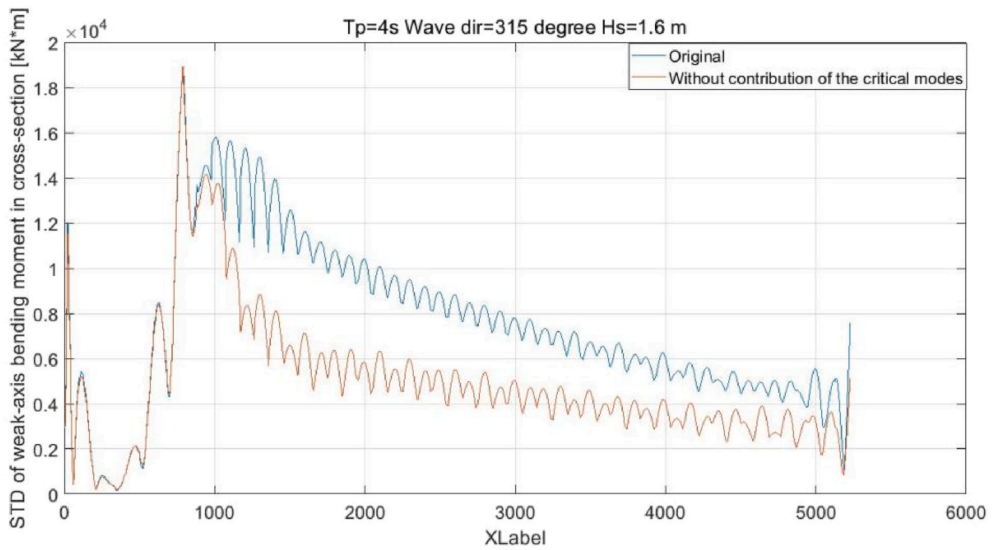


Fig. B5. Comparison of standard deviation of weak axis bending moments in cross-sections on the girder with and without contribution of the critical mode shapes, for $T_p = 4s$, $H_s = 1.6 m$, 315° wave direction. The blue line includes all of the vibrations modes while the red line excludes the contribution of all identified non-critical modes.

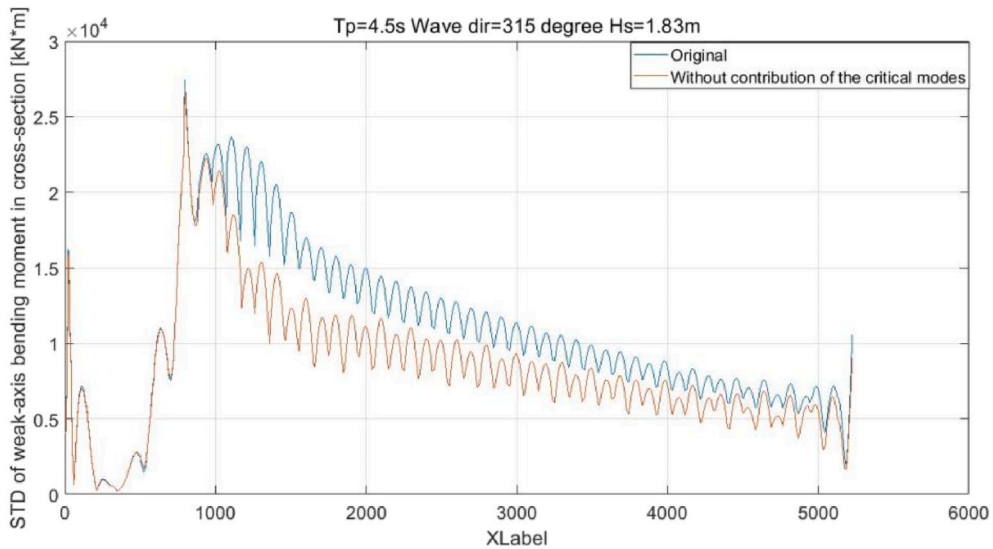


Fig. B6. Comparison of standard deviation of weak axis bending moments in cross-sections on the girder with and without contribution of the critical mode shapes, for $T_p = 4.5s$, $H_s = 1.83\text{ m}$, 315° wave direction. The blue line includes all of the vibrations modes while the red line excludes the contribution of all identified non-critical modes.

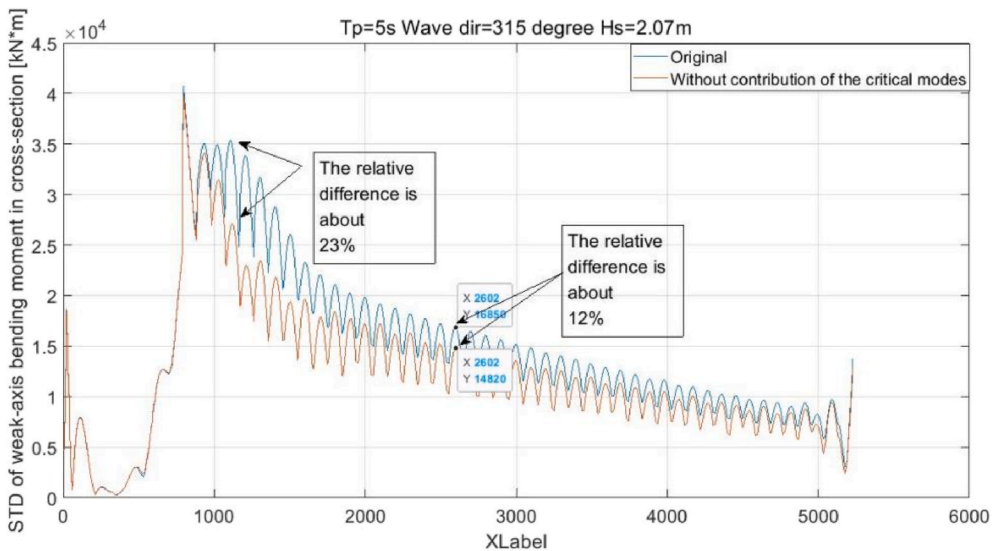


Fig. B7. Comparison of standard deviation of weak axis bending moments in cross-sections on the girder with and without contribution of the critical modes, for $T_p = 5s$, $H_s = 2.07\text{ m}$, 315° wave direction. The blue line includes all of the vibrations modes while the red line excludes the contribution of all identified non-critical modes.

The results in **Figures B5-B7** show that the relative importance of the contribution of the critical modes tends to decrease with the increase of T_p , while the extreme responses tend to increase with the increasing T_p . In addition, the 100-year contour line shows that H_s increases with the increase of T_p .

The most critical responses are observed in **Figure B7**. As shown in **Figure B7**, the critical modes might provide 23% of the STD of the dynamic response.

Power spectra of weak axis bending moment at cross-section at $x = 2611\text{ m}$ with and without contribution of the critical modes are compared in **Figure B8**. The major difference comes from the frequency components in between of 1.3 rad/s and 2 rad/s , while the study in the present paper shows that elementary beam theory tends to over-predict natural frequencies of the critical modes compared to shell element models for which shear lag effect has been accounted for. The impact of the over-prediction on extreme responses is related to natural frequencies of the critical modes and frequency distribution of damping and excitation loads. Therefore, the impact has to be judged case by case.

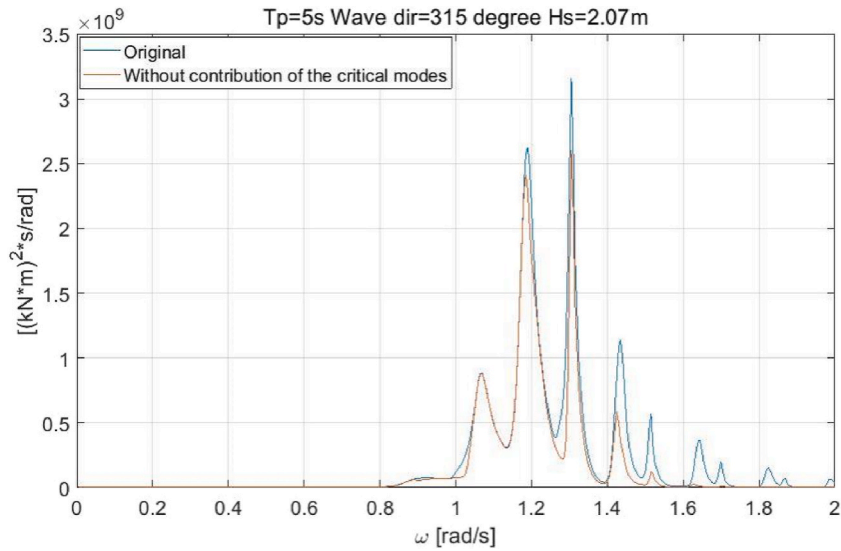


Fig. B8. Comparison of power spectra of weak axis bending moment at cross-section at $x = 2611$ m with and without contribution of the critical modes s , for $T_p = 5$ s, $H_s = 2.07$ m, 315° wave direction. The blue line includes all of the vibrations modes while the red line excludes the contribution of all identified non-critical modes.

Appendix C. Static analysis for shear lag effect in the reference structure subjected to inertial loads

Distribution of the inertial loads on the span is determined by the excited mode shape. However, fortunately, as linear finite element system is used, bending moment distribution induced by inertial load with a given distribution could be conveniently obtained by superimposing bending moment distribution induced by corresponding loads. Consequently, shear lag effect on bending moment distribution of a single span subjected to a line load on an arbitrary lateral diaphragm has been studied. Some selected representative results, i.e. MSC01, MSC02 and their corresponding beam element models (MSC01 and MSC02), are discussed as following. MSC01 and MSC02 are shell models for which upward uniformly distributed line loads are applied on the diaphragms located at $x = 16$ m and $x = 84$ m in the global coordinate system respectively. The models are described in Section 2.4.1.

Comparison of the results of MBC01 and MSC01 is shown in Figure C1. It shows that shear lag effect could result in 9% relative difference in critical weak axis bending moment which is in an end cross-section of the span. We denote the difference between MBC01 and MSC01 as $D^{C01}(x)$. As shown in Figure C1, $D^{C01}(x)$ could approximately be expressed as a linear function with an offset, see Eq. (C1), where k is the slope and b is the offset.

The line load in MSC02 is a mirror of the line load in MSC01 with respect to the diaphragm at $x = 50$ m while the rest part of MSC01 and MSC02 are identical. This means the difference between MSC02 and MBC02 (denoted as D^{C02}) is a mirror of D^{C01} with respect to the same plane at $x = 50$ m, see Eq. (C2). Consequently, when the bending moments in MSC01 and MSC02 are superimposed, shear lag effect induced difference in bending moment distribution could be significantly reduced to $2b$ which is a constant value along the span of the girder.

This fact means, when the boundary condition and the applied loads of a part of girder is symmetrical, the difference of weak axis bending moment between the shell and beam models could be a constant value. This difference indicates that the cross-sectional stiffness of the model in cross-sections at the two ends of the model is affected by shear lag effect induced by the applied loads. In addition, this fact also gives an explanation of the difference between MSA01 and MBA01, for which a single span is subjected to self-weight while the difference is a very small value and approximately constantly distributed. While the observations are agreed by the analytical analysis given in [31].

$$D^{C01}(x) = k(x - 50) + b \tag{c1}$$

$$D^{C02}(x) = -k(x - 50) + b \tag{c2}$$

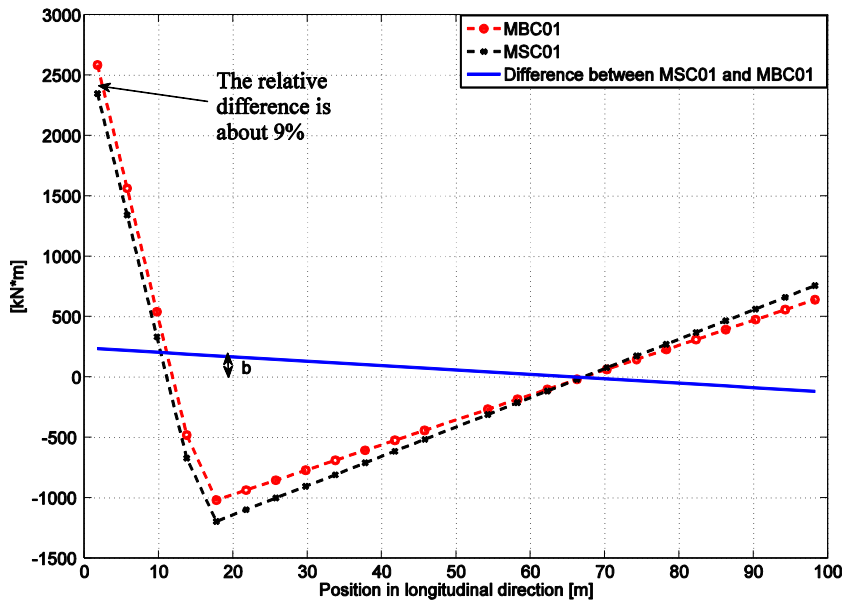


Fig. C1. Comparison of bending moments in cross-sections of a single span girder subjected to a line load on a lateral diaphragm given by shell and beam models (MSC01 and MBC01 described in Section 2.4).

Appendix D. Static analysis for trend of influence of configuration of a reference girder on shear lag effect

Trend of influence of configuration of a reference girder on shear lag effect is analyzed in this appendix by comparing bending moment distribution in a single span of the girder simulated by several beam and shell models with different ratio between span length and width (L/B) and subjected to static loads. The models are described in Section 2.4.

MSD01 and MSD02 are shell element models which are identical to MSC01 except that the girder width is reduced from 27.6 m to 13.8 m and 0.5 m respectively; while, to make the results of the models be comparable, we make resultants of each of the line loads on the lateral bulkheads of the models identical. Consequently, the models could be classified into three groups with the same ratio between span length and height ($L/H = 31.75$) but different ratio between girder width and height, i.e. $B/H = 8.76$, $B/H = 4.38$, and $B/H = 0.16$. By fixing the height, these three groups have different L/B , i.e. $L/B = 3.62$, $L/B = 7.24$, and $L/B = 198$. It could be observed that shear lag effect on bending moment distribution is reduced by reducing the B/H , for instance the difference between MSD02 and MBD02, for which $B/H = 0.16$, are negligible. This trend agrees with the trend of shear lag effect on the corresponding stress distribution with respect to variation of B/H . This agreement supports that the differences in the bending moments given by the corresponding beam and shell models come from shear lag effect. The same conclusion is achieved by comparing MSB01, MSD03 and their corresponding beam element models. MSB01 and MSD03 are shell element models of a single span subjected to self-weight. MSD03 is identical to MSB01 except that the girder width is reduced to from 27.6 m to 0.5 m. In addition, a sensitivity study shows that numerical issues, such as different numerical approaches for the boundary condition of the analyzed models, have negligible effect on the bending moment distributions discussed in this appendix.

To shed light on effect of L/H on the difference in weak axis bending moment distribution, MSD04 and MSD05 are developed by increasing the span length of MSC01 ($B/H = 8.76$) and MSD01 ($B/H = 4.38$) from 100 m to 200 m respectively (the L/H is doubled to 63.50). It should be noted that, as shown in Table 1, the position of the applied loads have been adjusted correspondingly to make the models be comparable. Comparisons of these models and their corresponding beam element models show, for a given value of B/H , the difference could be reduced by increasing the value of L/H .

Effects of the thickness of the plates and bulkheads (t) and distance between two lateral bulkheads (d_{bk}) on the bending moment distribution have been analyzed as well. Within a realistic range, the effects of t and d_{bk} are negligible.

References

- [1] Npra. <https://www.vegvesen.no/en/roads/Roads+and+bridges/Road+projects/e39coastalhighwayroute>. [Accessed 3 April 2019].
- [2] Moan T, Eidem ME. In: Wang CM, Lim SH, Tay ZY, editors. Floating bridges and submerged tunnels in Norway—the history and future outlook”. WCFSS2019, lecture notes in civil engineering, vol. 41. Springer Nature Singapore; 2020. https://doi.org/10.1007/978-981-13-8743-2_5.
- [3] Kvåle KA, Sigbjørnsson R, Øiseth O. Modelling the stochastic dynamic behaviour of a pontoon bridge: a case study. *Comput Struct* 2016;165:123–35.
- [4] Watanabe E. Floating bridges: past and present. *Struct Eng Int* 2003;13(2):128–32.
- [5] HistoryLink. <https://historylink.org/ContactUs>. [Accessed 3 April 2019].
- [6] Npra. <https://www.vegvesen.no/Europaveg/e39stordos/fjordkryssing-bjornafjorden>. [Accessed 3 April 2019].

- [7] EN 1993-1-5. Eurocode 3: Design of steel structures - Part 1-5: General rules - Plated structural elements 2006.
- [8] Standards Norway. Design of steel structures. Standards Norway: NORSOK STANDARD N-004; 2004.
- [9] Sbj-32-C3-Svv-90-Ba-001. Design basis Bjørnafjorden floating bridges. Statens vegvesen; 2017.
- [10] Chen Z, Xu Y, Xia Y, Li Q, Wong K. Fatigue analysis of long-span suspension bridges under multiple loading: case study. *Eng Struct* 2011;33(12):3246–56.
- [11] Zhu Q, Xu Y, Shum K. Stress-level buffeting analysis of a long-span cable-stayed bridge with a twin-box deck under distributed wind loads. *Eng Struct* 2016;127: 416–33.
- [12] Kong X, Wu D, Cai C, Liu Y. New strategy of substructure method to model long-span hybrid cable-stayed bridges under vehicle-induced vibration. *Eng Struct* 2012;34:421–35.
- [13] Li Z, Zhou T, Chan T, Yu Y. Multi-scale numerical analysis on dynamic response and local damage in long-span bridges. *Eng Struct* 2007;29(7):1507–24.
- [14] Ding Y, Li A, Du D, Liu T. Multi-scale damage analysis for a steel box girder of a long-span cable stayed bridge. *Structure and Infrastructure Engineering* 2010;6 (6):725–39.
- [15] Luan C, Gao Z, Moan T. Development and verification of a time-domain approach for determining forces and moments in structural components of floaters with an application to floating wind turbines. *Mar Struct* 2017;51:87–109. <https://doi.org/10.1016/j.marstruc.2016.10.002>.
- [16] Luan C, Gao Z, Moan T. Comparative analysis of numerically simulated and experimentally measured motions and sectional forces and moments in a floating wind turbine hull structure subjected to combined wind and wave loads. *Eng Struct* 2018;177:210–33. <https://doi.org/10.1016/j.engstruct.2018.08.021>.
- [17] Cheng Z, Gao Z, Moan T. Numerical modeling and dynamic analysis of a floating bridge subjected to wind, wave, and current loads. *J Offshore Mech Arctic Eng* 2019;141:011601.
- [18] Marintek. SIMO User's Manual 2011.
- [19] Marintek. RIFLEX User's Manual 2013.
- [20] Orcina. Orcaflex documentation. 2018. <https://www.orcina.com/SoftwareProducts/OrcaFlex/Documentation/index.php>. [Accessed 8 December 2019].
- [21] Viuff T, Xiang X, Leira B, Øiseth O. Code-to-code verification of end-anchored floating bridge global analysis. In: Proceedings of 37th international conference on ocean, offshore and arctic engineering. OMAE2018; 2018. Madrid, Spain.
- [22] Viuff T, Xiang X, Leira B, Øiseth O. Effects of wave directionality on extreme response for a long end-anchored floating bridge. *Appl Ocean Res* 2019;90:101843.
- [23] Cheng Z, Gao Z, Moan T. Wave load effect analysis of a floating bridge in a fjord considering inhomogeneous wave conditions. *Eng Struct* 2018;163:197–214.
- [24] Cheng Z, Gao Z, Moan T. Hydrodynamic load modeling and analysis of a floater bridge in homogeneous wave conditions. *Mar Struct* 2018;59:122–41.
- [25] Lin Z, Zhao J. Least-work solutions of flange normal stresses in thin-walled flexural members with high-order polynomial. *Eng Struct* 2011;33:2754–61.
- [26] Moffatt K, Dowling P. Shear lag in steel box girder bridges. *Struct Eng* 1975;53:439–48.
- [27] Lertsima C, Chaisomphob T, Yamaguchi E. Stress concentration due to shear lag in simply supported box girders. *Eng Struct* 2004;26:1093–101.
- [28] Zhou S. Finite beam element considering shear lag effect in box girder. *J Eng Mech* 2010;136:1115–22.
- [29] Wu Y, Liu S, Zhu Y, Lai Y. Matrix analysis of shear lag and shear deformation in thin-walled box beams. *J Eng Mech* 2003;129:944–50.
- [30] Cambronero-Barrientos F, Díaz-del-Valle J, Martínez-Martínez J-A. Beam element for thin-walled beams with torsion, distortion, and shear Lag. *Eng Struct* 2017;143:571–88.
- [31] Luo Q, Wu Y, Tang J, Li Q. Experimental studies on shear lag of box girders. *Eng Struct* 2002;24:469–77.
- [32] Reissner E. Analysis of shear lag in box beams by the principle of minimum potential energy. *Q Appl Math* 1946;63:268–78.
- [33] Sedlacek G, Bild S. A simplified method for the determination of the effective width due to shear lag effects. *J Constr Steel Res* 1993;24:155–82.
- [34] SBJ-30-C3-NOR-90-RE-100. K7 Bjørnafjorden End-anchored floating bridge Summary report. Norconsult; 2017.
- [35] SBJ-31-C3-MUL-22-RE-100. Bjørnafjorden, straight floating bridge phase 3 Analysis and design (Base Case). Multiconsult; 2017.
- [36] SBJ-30-C3-NOR-90-RE-101. K7 bjørnafjorden end-anchored floating bridge appendix A – drawings binder. Norconsult; 2017.
- [37] Al-Sherrawi MHM, Fadhil GH. Effect of stiffeners on shear lag in steel box girders. *Ahmed Fadhil Al-Khwarizmi Engineering Journal* 2012;8(2):63–76.
- [38] DNVGL. Genie user manual. 2019.
- [39] DNVGL. Sestra user manual. 2019.
- [40] Smith M. ABAQUS/Standard user's manual, version 6.9. Providence, RI: Dassault Systèmes Simulia Corp.; 2009.
- [41] Faltinsen OM. Sea loads on ships and offshore structures. UK: Cambridge University Press; 1990.
- [42] Naess A, Moan T. Stochastic dynamics of marine structures. UK: Cambridge University Press; 2013.
- [43] Vika E. Modelling and analysis of a floating bridge, master thesis. Trondheim: Norwegian University of Science and Technology; 2018.
- [44] Kvåle KA, Øiseth O, Rønning A. Operational modal analysis of an end-supported pontoon bridge. *Eng Struct* 2017;148:410–23. <https://doi.org/10.1016/j.engstruct.2017.06.069>.
- [45] Brownjohn JMW, Magalhães F, Caetano E, Cunha A. Ambient vibration retesting and operational modal analysis of the Humber Bridge. *Eng Struct* 2010;32: 2003–18. <https://doi.org/10.1016/j.engstruct.2010.02.034>.
- [46] Magalhães F, Cunha A, Caetano E. Dynamic monitoring of a long span arch bridge. *Eng Struct* 2008;30:3034–44. <https://doi.org/10.1016/j.engstruct.2008.04.020>.
- [47] Cheng Z, Gao Z, Moan T. Extreme responses and associated uncertainties for a long end-anchored floating bridge. *Eng Struct* 2020;219:110858.
- [48] Cheng Z, Svangstu E, Moan T, Gao Z. Long-term joint distribution of environmental conditions in a Norwegian fjord for design of floating bridges. *Ocean Eng* 2019;191:106472.
- [49] Cheng Z, Svangstu E, Moan T, Gao Z. Assessment of inhomogeneity in environmental conditions in a Norwegian fjord for design of floating bridges. *Ocean Eng* 2021;220:108474.